Biogeosciences Discuss., https://doi.org/10.5194/bg-2018-78
Manuscript under review for journal Biogeosciences
Discussion started: 10 April 2018

Reviews and syntheses: ^{210}Pb-derived sediment and carbon accumulation rates in vegetated coastal ecosystems: setting the record straight

Ariane Arias-Ortiz[1*], Pere Masqué[1,2,3,4], Jordi Garcia-Orellana[1,2], Oscar Serrano[3], Inés Mazarrasa[5], Núria Marbà[6], Catherine E. Lovelock[7], Paul Lavery[3,8] and Carlos M. Duarte[9]

[1]Institut de Ciència i Tecnologia Ambientals, Universitat Autònoma de Barcelona, Bellaterra, 08193 Barcelona, Spain.
[2]Departament de Física, Universitat Autònoma de Barcelona, Bellaterra, 08193 Barcelona, Spain.
[3]School of Science, Edith Cowan University, 270 Joondalup Drive, Joondalup WA 6027, Australia.
[4]UWA Oceans Institute & School of Physics, The University of Western Australia, 35 Stirling Highway, Crawley 6009, Australia.
[5]Environmental Hydraulics Institute "IH Cantabria", Universidad de Cantabria, C/ Isabel Torres N◦15, Parque Científico y Tecnológico de Cantabria, 39011, Santander, Spain.
[6]Department of Global Change Research. IMEDEA (CSIC-UIB) Institut Mediterrani d'Estudis Avançats, C/ Miguel Marqués 21, 07190 Esporles (Mallorca), Spain.
[7]School of Biological Sciences, The University of Queensland, St Lucia, QLD 4072, Australia.
[8]Centro de Estudios Avanzados de Blanes, Consejo Superior de Investigaciones Científicas. Blanes, Spain 17300.
[9]King Abdullah University of Science and Technology (KAUST), Red Sea Research Center (RSRC), Thuwal, 23955-6900, Saudi Arabia.

Correspondence to: Ariane Arias-Ortiz (ariane.arias@uab.cat)

Abstract. Vegetated coastal ecosystems, including tidal marsh, mangrove and seagrass, are being increasingly assessed for their potential in carbon dioxide sequestration worldwide. However, there is a paucity of studies that have effectively estimated the accumulation rates of sediment organic carbon (C_{org}) beyond the mere quantification of C_{org} stocks. Here, we discuss the use of the ^{210}Pb dating technique as a practical tool to measure the rate of C_{org} accumulation in vegetated coastal ecosystems. We critically review the status of ^{210}Pb dating methods of vegetated coastal sediments and assess the limitations that apply to these ecosystems, which are often composed by heterogeneous sediments, abundant in coarse particles, with varying inputs of organic material, and are disturbed by natural and anthropogenic processes causing sediment mixing, changes in sedimentation rates or erosion. Through a range of simulations, we discuss the most relevant processes that impact the ^{210}Pb record in vegetated coastal ecosystems and evaluate the deviations in sediment and C_{org} accumulation rates produced by anomalies in ^{210}Pb profiles. Our results show that the deviation in the determination of sediment and derived C_{org} accumulation rates is within 20% confirming that the ^{210}Pb dating technique is secure. However, while these uncertainties might be acceptable for the determination of mean sediment and C_{org} accumulation rates over the last century, they may not always allow the determination of a detailed geochronology, historical reconstruction, or to ascertain rates of change and fluxes. Additional tracers or geochemical data need to be used in concert to constrain the ^{210}Pb-derived results and to properly interpret the processes recorded in vegetated coastal sediments. The framework provided in this study can be

instrumental in reducing the uncertainties associated to the estimates of C_{org} accumulation rates in vegetated coastal sediments.

Keywords: ^{210}Pb, vegetated coastal sediments, carbon accumulation rates, sediment dating, blue carbon.

1 Introduction

Recognition of the globally significant role of vegetated coastal habitats, including tidal marsh, mangrove and seagrass, as sinks of carbon dioxide (CO_2) (Duarte et al., 2013) has led to a rapid growth in the interest to evaluate the amount of organic carbon (C_{org}) these ecosystems sequester, in order to quantify the potential to mitigate CO_2 emissions through their management in an approach described as "*Blue Carbon*" (Duarte et al., 2013; Mcleod et al., 2011; Nellemann et al., 2009). However, efforts to include vegetated coastal ecosystems into existing carbon mitigation strategies have met with an important limitation: there is a paucity of estimates of C_{org} sequestration rates, a growing concern especially within the seagrass research community, where the paucity of estimates is greatest (Johannessen and Macdonald, 2016, 2018; Macreadie et al., 2018).

Two interrelated measurements of importance to this sequestration are the sediment C_{org} density and the sedimentation velocity or sedimentation rate. To date, most of the research has focused in the first term, which informs about the C_{org} stock sequestered in sediments (Howard et al., 2014), indicating that between 50% and 90% of C_{org} stock in vegetated coastal ecosystems is found in their sediments (Pendleton et al., 2012). However, C_{org} stocks alone cannot be used to fully assess carbon storage or establish comparisons among sites. Measurements of sedimentation rates and derived C_{org} accumulation rates address the question of how much carbon is sequestered in a specified time period and the quantification of the ongoing sink capacity. In general, C_{org} accumulation rates are obtained by measuring the concentration of C_{org} in sediments and ascribing dates to either the entire profile of interest or to specific intervals. Determination of mean C_{org} accumulation rates is partially dependent on the time scale of interest and the dating methods used. ^{210}Pb has been shown to be an ideal tracer for dating aquatic sediments deposited during the last 100 yr: 1) providing a time frame compatible with management actions (C_{org} requires a minimum permanence of approximately 40-150 years to be considered relevant for climate change mitigation; Marland et al., 2001); 2) ^{210}Pb is not affected by interannual variability (C_{org} that naturally cycles through an ecosystem is part of the "baseline" condition; Howard et al., 2017); and 3) it enables the determination of sediment accumulation rates and changes which have occurred during the last century, the period of greatest human influence on the environment (Duarte, 2014). Although several review papers have been published in recent years which have elaborated the various applications of excess ^{210}Pb as a tracer in terrestrial and aquatic environments (Appleby, 2001; Baskaran et al., 2014; Du et al., 2012; Kirchner and Ehlers, 1998; Mabit et al., 2014; Sanchez-Cabeza and Ruiz-Fernández, 2012; Smith, 2001), little attention has been paid to the potential limitations of the ^{210}Pb dating method in vegetated coastal sediments.

^{210}Pb ($T_{1/2}$ = 22.3 yr) is part of the ^{238}U decay series. In coastal sediments, the presence of ^{210}Pb has two different origins: the supported ^{210}Pb derived from the *in-situ* decay of ^{226}Ra in the sediment matrix and the excess ^{210}Pb, delivered to the surface of sediments as a result of ^{222}Rn decay in the atmosphere. ^{210}Pb is particle-reactive in the marine environment, hence, once it reaches surface waters it rapidly settles in the sediment bound to particulate matter (Robbins, 1978). The ^{210}Pb-derived sedimentation rate is obtained from the profile generated by radioactive decay of the excess ^{210}Pb buried in the sediment (0.0311 yr^{-1}), which is supplied at a supposedly constant rate (Fig. 1).

Vegetated coastal ecosystems may act as closed systems where the sediment accumulation is mainly associated with the build-up of autochthonous organic and inorganic material (McKee, 2011). In this situation, excess ^{210}Pb is deposited under ideal conditions, primarily from atmospheric fallout at steady state, with no post depositional mobility except for physical or biological mixing of the sediments (e.g. Alongi et al., 2004; Cochran et al., 1998; Marbà et al., 2015). In some cases, however, the process responsible for incorporating excess ^{210}Pb into the sediments might be more complex. Vegetated coastal ecosystems, may receive both autochthonous and allochthonous sediments from the upstream catchment, coastal erosion or from the offshore zone during storm events (Turner et al., 2007), or in response to land use change disturbances (Mabit et al., 2014; Ruiz-Fernández and Hillaire-Marcel, 2009). The bottom sediments might be reworked through the action of tides, currents, and waves as well as through boat anchoring, dredging or fishing activities (e.g. Mazarrasa et al., 2017; Sanders et al., 2014; Serrano et al., 2016; Smoak et al., 2013). Effects associated with climate change such as sea level rise and extreme climatic events may also have an impact on rates of production and decomposition of organic matter (OM) and on sediment and C_{org} accumulation (Alongi et al., 2008; Mudd et al., 2010). In this event, although the direct atmospheric supply might be the dominant process determining concentrations of excess ^{210}Pb, sediment redistribution processes and complex accretion dynamics may violate some of the assumptions of ^{210}Pb dating models, producing anomalous ^{210}Pb profiles that are difficult to interpret.

Sediments of vegetated coastal ecosystems are known to be heterogeneous, consisting of coarse grained sediments or bedrock covered by deposits of fine grained sediments that settled down as vegetation established (McGlathery et al., 2012; Olff et al., 1997). The percentage of living (e.g. roots) and recently formed organic material is greatest in the upper 10 cm and may be affected by varying inputs of detrital sediment within vegetated coastal ecosystems and by its relative rate of decomposition. While tidal marsh and mangrove sediments have relatively high organic matter content (on average 25%) (Breithaupt et al., 2012; Cochran et al., 1998), mineral deposits account for the majority (>85%) of the accumulated substrate in seagrass sediments (Koch, 2001; Mazarrasa et al., 2015) (Table 1). Excess ^{210}Pb has a strong affinity for surface particles of fine sediments (Chanton et al., 1983; Cundy and Croudace, 1995; He and Walling, 1996a) and organic matter (Wan et al., 2005), thus any changes in these parameters due to sediment redistribution processes or to natural heterogeneity may also result in unique types of ^{210}Pb concentration profiles in sediment cores of vegetated coastal ecosystems, adding complexity to the determination of sediment model age and sedimentation rates.

Biogeosciences Discuss., https://doi.org/10.5194/bg-2018-78
Manuscript under review for journal Biogeosciences
Discussion started: 10 April 2018

Here, we provide a critical review of the current status of ^{210}Pb dating methods of vegetated coastal sediments and assess the limitations that apply to ^{210}Pb dating of cores in such ecosystems. We use a set of practical approaches, based on examples from the literature and numerical simulations, to discuss the basic processes involved in the depth distribution of excess ^{210}Pb in vegetated coastal sediments and present how anomalies on these profiles affect estimated sediment and C_{org} accumulation rates. We also provide guidance on complementary analyses to accompany the ^{210}Pb dating technique that can enhance sediment and derived C_{org} accumulation rates estimates.

2 Methods

2.1 Bases of the ^{210}Pb dating methodology

^{210}Pb-derived sediment chronologies are based in the interpretation of the rate of decline of excess ^{210}Pb concentration with depth in a sediment core. Excess ^{210}Pb concentrations are determined by subtracting supported ^{210}Pb (taken as in equilibrium with ^{226}Ra) to total ^{210}Pb concentrations (for a detailed description of the laboratory analysis of these radioisotopes see Du et al., 2012). The distribution of excess ^{210}Pb in the sediment can be described as:

$$\frac{\partial \rho C}{\partial t} = \frac{\partial}{\partial z} \cdot \left(D\rho \frac{\partial C}{\partial Z} \right) - \frac{r\, \partial \rho C}{\partial z} - \lambda \rho C \qquad \text{(Eq. 1)}$$

where ρ is sediment bulk density (g cm^{-3}), C is the concentration of excess ^{210}Pb (Bq kg^{-1}), z is depth below the sediment–water interface (cm), D is a coefficient characterizing the sediment mixing rate (cm^{2} yr^{-1}), r is the sedimentation rate (cm yr^{-1}), λ is the ^{210}Pb decay constant and t is time. Throughout this manuscript depth (z) is represented as mass depth (m) to correct for compaction. Mass depth (g cm^{-2}) results from the multiplication of $z \cdot \rho$, and sedimentation rates are expressed as mass accumulation rates (MAR) in g cm^{-2} yr^{-1}, which can be described as $MAR = \rho(v + q)$ with v and q the accretion and compaction velocities, respectively (Abril, 2003b) (Eq.2).

$$\frac{\partial A}{\partial t} = \frac{\partial}{\partial m} \left(k_m \frac{\partial A}{\partial m} \right) - MAR \frac{\partial A}{\partial m} - \lambda A \qquad \text{(Eq. 2)}$$

where A is the specific activity of ^{210}Pb (Bq cm^{-2}) and k_m an effective mixing coefficient (g^{2} cm^{-4} yr^{-1}).

The ^{210}Pb technique was first applied by Koide et al. (1972) to date marine sediments. Since then, a family of dating models has been used to interpret the excess ^{210}Pb depth distribution in marine and freshwater sediment cores, increasing in variety and complexity and involving a large diversity of post-depositional redistribution processes (Table 2). However, the three most classic ^{210}Pb dating models are 1) the Constant Initial Concentration model (CIC) (Robbins, 1978); 2) the Constant Flux: Constant Sedimentation (CF:CS) model (Krishnaswamy et al., 1971); and 3) the Constant Rate of Supply (CRS) model (Appleby and Oldfield, 1978). A literature search in the Web of Science^{TM} (accessed October 25, 2017) with the keywords “mangrove sediment", "salt marsh/tidal marsh sediment", "seagrass sediment” AND “^{210}Pb” produces 70, 150 and 20 results, respectively, all of them using one or more of the above dating models. These approaches share a set of assumptions: (1) the deposition of excess ^{210}Pb is at steady state, (2) there is no post depositional mobility of ^{210}Pb except for physical or biological mixing of the sediments, (3) the deposition of excess ^{210}Pb is ideal, i.e., new radioactive inputs will be deposited above the previously existing material, and (4) the sedimentary sequence is continuous. The CIC model assumes that the initial concentration of excess ^{210}Pb at the sediment-water interface is constant with time and that the excess ^{210}Pb flux co-varies with MAR. This model permits estimation of the age at any depth where ^{210}Pb has been measured and thus estimation of the corresponding sedimentation history (see Table 2). In active and complex systems, however, sediment disturbances or changes in the deposition dynamics cause variations in the initial excess ^{210}Pb concentration, resulting in age reversals down core that prevent the construction of an age model. Based in our experience, the existence of unaltered sedimentary records in vegetated coastal ecosystems is rare (Swales and Bentley, 2015), and therefore the CIC model was not considered in this study.

The Constant Flux: Constant Sedimentation (CF:CS) model (Krishnaswamy et al., 1971) assumes that the sedimentation rate does not vary with time. Then, the specific excess ^{210}Pb activity (C_0: Bq kg^{-1}) of freshly deposited material is constant initially and decreases exponentially with depth. If mixing is negligible or there is a constant mixing coefficient (k_m) at the surface mixed layer of the core, *MAR* is constant and can be calculated from the excess ^{210}Pb concentration profile below the surface mixed layer. This model is used also when concentrations of excess ^{210}Pb decline piecewise, showing two or more exponentially decaying segments. Then, mean *MAR* can be derived for each segment (Goldberg et al., 1977).

The CRS model assumes that the flux of excess ^{210}Pb onto the sediment–water interface is constant over time. The dating is based on the comparison of excess ^{210}Pb inventories (A_m; Bq m^{-2}) below a given depth (integration of excess ^{210}Pb activity as a function of the mass depth) with the overall excess ^{210}Pb inventory in the sediment core (I). The accurate estimation of the total ^{210}Pb inventory is of critical importance for the application of the CRS model (Appleby, 2001). Variations in A_m/I are related to variations in S (see Table 2). When excess ^{210}Pb fluxes and S are both constant, the CRS and CIC models converge to the CF:CS model (Table 2). For further description of the models and the associated equations see references in Table 2 or Appleby (2001).

Once the dating model is established, the C_{org} accumulation rate (C_{acc}-MAR) can be obtained as the product of the fraction of %C_{org} accumulated over a period of time *(t)* by the MAR of that period, derived from ^{210}Pb age model:

$$C_{org-MAR} = \frac{\sum_{n=i}^{t} (\%C_{org_i} \cdot m_i)}{m_t} \cdot MAR_t \quad \text{(Eq. 3)}$$

where $(\%C_{orgi} \cdot m_i)$ is the mass per unit area of C_{org} at layer i (g C_{org} m^{-2}), m_t is the total cumulative mass over the period (t) (g m^{-2}) and MAR_t is the mass accumulation rate of the period of interest (g m^{-2} yr^{-1}).

2.2 Numerical simulations

We performed a literature review of studies on sediment accumulation in vegetated coastal ecosystems to identify the most common sedimentary processes that result in anomalous types of excess ^{210}Pb concentration profiles with depth (Fig. 2).

These could be summarized in five main processes: mixing, increasing sedimentation, erosion, changes in sediment grain size, and decay of organic matter (OM). Then, we simulated the target processes on initial undisturbed seagrass, mangrove and tidal marsh sediments to determine the potential deviations (defined as the difference between the value which has been computed and the correct value) in C_{org}-MAR and explain the limitations of the ^{210}Pb dating technique in these ecosystems. All simulations started from an ideal excess ^{210}Pb profile, complying with all assumptions, that was then manipulated to reflect the potential effect of each process. The ideal excess ^{210}Pb profiles was modelled considering the following: (1) a constant flux of excess ^{210}Pb (Φ) of 120 Bq m^{-2} yr^{-1} i.e., the average global atmospheric flux reported by Preiss et al. (1996); (2) a MAR of 0.2 g cm^{-2} yr^{-1} and dry bulk density (DBD) of 1.03 g cm^{-3} to represent seagrass sediments; and (3) a MAR of 0.3 g cm^{-2} yr^{-1} and DBD of 0.4 g cm^{-3} to represent mangrove/tidal marsh sediments based on typical values representative of these ecosystems (Duarte et al. 2013) (Table 1). Simulated surface specific activity of excess ^{210}Pb ($A_{0;}$ in Bq m^{-2}) in ideal profiles was estimated through equation 4. Then equation 5 was applied to estimate excess ^{210}Pb specific activities along the ideal profile (Supplementary, Table 1).

$$A_0 = \frac{\Phi}{\lambda}\left(1 - e^{-\lambda^{m_0}/_{MAR}}\right) \tag{4}$$

$$A_m = A_0 \cdot e^{-\lambda^{m}/_{MAR}} \tag{5}$$

Activities of excess ^{210}Pb per unit area *(A_m)* were then converted to concentrations, C_m in Bq kg^{-1}, by dividing A_m by the cumulative mass *(m)* at each layer. Ideal profiles were then altered to simulate the following processes/scenerios: mixing, increasing sedimentation, erosion, changes in sediment grain size and OM decay. See Table 3 for a summary description of the modeled scenarios and refer to appendix A for a detailed description of the methodology used to conduct each simulation.

The CF:CS and CRS dating models were applied to altered excess ^{210}Pb profiles to determine MAR and subsequently C_{org}-MAR rates through equation 3 assuming average sediment C_{org} contents of 2.5% and 8% in seagrass and mangrove/tidal marsh, respectively. Under ideal conditions C_{org}-MAR rates were 50 g C_{org} m^{-2} yr^{-1} and 240 g C_{org} m^{-2} yr^{-1}, respectively. While this overall model structure was used in all simulated scenarios, C_{org}-MAR rates under ideal conditions varied from those reported above (50 g C_{org} m^{-2} yr^{-1} and 240 g C_{org} m^{-2} yr^{-1}) in OM decay simulations where the initial sediment OM content was 16.5% and 65% (see appendix A).

3 Results and Discussion

3.1 Types of excess ^{210}Pb concentration profiles

Seven distinct types of excess ^{210}Pb concentration profiles can be identified in vegetated coastal sediments based on the literature (Fig. 2). Type I is produced by constant sediment accumulation in steady state conditions (i.e. 'ideal' profiles). The other six types of excess ^{210}Pb concentration profiles summarize the most common disturbances encountered in vegetated costal sediments that are related to the presence of mixing (physical or bioturbation), increasing sedimentation rates, erosion, or alteration by intrinsic features of sediments such as heterogeneous grain size distribution and decay of OM.

- Type II illustrates a moderate decrease in the slope of excess ^{210}Pb concentrations in the upper part of the sediment core, which is often related to higher sedimentation rates (Cearreta et al., 2002; Haslett et al., 2003; Swales and Bentley, 2015), but can also be related to mixing processes (Gardner et al. 1987).
- Type III, showing constant excess ^{210}Pb concentrations along the upper part of the core overlaying an exponential decaying trend, is usually interpreted as the outcome of intense mixing as a result of bioturbation or as sediment resuspension and re-deposition and rework (Sanders et al., 2010b; Serrano et al., 2016c; Sharma et al., 1987; Smoak and Patchineelam, 1999).
- Type IV profiles show a subsurface maximum of excess ^{210}Pb and have been attributed to a variety of factors. Similarly to type III, these profile types can be caused by mixing processes in vegetated coastal ecosystems (Sanders et al., 2010a; Serrano et al., 2016a; Yeager et al., 2012). However, they could also be produced by an acceleration of the sedimentation rate, as interpreted by Greiner et al. (2013), Smoak et al. (2013) and Bellucci et al. (2007) in seagrass, mangrove and tidal marsh, respectively, or by the decay of OM, as modeled by Chen and Twilley (1999) and Mudd et al. (2009), and observed by Church et al. (1981) in tidal marsh sediments containing > 30% OM in top layers. Additionally, type IV profiles could also be explained by non-ideal deposition (i.e. a fraction of the new excess ^{210}Pb input onto the sediment is not retained at the surface but penetrates to deeper layers), a process reported in peatlands and in sediments with very high porosities (> 90%) at the sediment-water interface (Abril and Gharbi, 2012; Olid et al., 2016).
- Type V profiles had scattered excess ^{210}Pb concentrations, which might reflect periodic repetition of processes that can cause type III or IV profiles and often are interpreted as evidence of repetitive reworking in the overall mixed sediment column (Serrano et al., 2016c; Smoak and Patchineelam, 1999). However, this profile form has also been explained by the deposition of excess ^{210}Pb outpacing its decay (λ = 0.03111 yr^{-1}) (Alongi et al., 2005) or by a heterogeneous grain-size sediment distribution with depth (Chanton et al., 1983; Kirchner and Ehlers, 1998; Sanders et al., 2010a), which could indicate varying excess ^{210}Pb fluxes due to flood events, major land use-changes or changes in vegetation cover (Appleby, 2001; Marbà et al., 2015)
- Types VI and VII represent low excess ^{210}Pb activities with depth, apparently showing low, negligible modern net accumulation of sediments. Such profiles are usually related to an abundance of coarse sediments or to erosion processes, as shown in tidal marsh sediments (Ravens et al., 2009) and bare sediments that were previously vegetated with seagrass in Greiner et al. (2013), Marbà et al. (2015) and Serrano et al. (2016c).

Our literature review reveals that various sedimentary processes might produce similar types of excess ^{210}Pb concentration profiles. Any type of excess ^{210}Pb concentration profile has several numbers of mathematical modelling approaches (see below), which lead to development of differing chronologies and sedimentation histories. Hence the knowledge of the process causing variation in the excess ^{210}Pb record aids in the determination of the sediment and C_{org} accumulation rates.

3.2 Simulated sediment and C_{org} accumulation rates (MAR and C_{org}-MAR)

We ran simulations for sedimentary processes (mixing, enhanced sedimentation, erosion) and heterogeneous sediment composition (grain size distribution and OM decay). Results of the modelled excess ^{210}Pb profiles are summarized in Figures 3 and 4. We estimated sediment and C_{org}-MAR for the simulated profiles by applying the CF:CS and CRS models, and results were compared with those from their respective ideal non-disturbed ^{210}Pb profiles. The estimated deviations in accumulation rates from those expected under ideal conditions are shown in Figure 5 for seagrass and mangrove/tidal marsh ecosystems.

3.2.1 Mixing

Simulations of surface mixing (A and B, Fig. 3a) yielded ^{210}Pb concentrations profiles similar to types II and III (Fig.2), while deep mixing (scenario C) led to stepwise excess ^{210}Pb profile forms similar to type V. Calculated MAR and C_{org}-MAR deviated 0 to 10% from the expected value in seagrass sediments, while deviations were negligible (<2%) in mangrove/tidal marsh sediments (Fig. 5). In both cases, higher deviations from the expected rates were associated with the CF:CS model, since this model interprets any divergence from the 'ideal' exponential decrease of the excess ^{210}Pb concentration with depth to reflect random variation. In contrast, the CRS model is based on the excess ^{210}Pb inventory (I), that is unaffected by vertical mixing. Mixing will have a significant effect on dates in the CRS model in the event that the thickness of the mixed layer exceeds 15% of the depth of the excess ^{210}Pb profile (Oldfield and Appleby, 1984).

3.2.2 Increasing sedimentation rates

Simulated increases in sedimentation rates from 20% to 300% (scenarios D to G, Fig. 3b) resulted in similar profile forms than those of surface mixing. Increases in sedimentation rates were modeled over the last 30 yr, a period over which more than a 2-fold increase was needed to produce a reversal of excess ^{210}Pb concentrations with depth such as in type IV profiles (Fig. 2). Generally, the influence of change in the sedimentation rate was better captured with the CRS model. The CF:CS model, in contrast, failed to account for rapid increases in sedimentation rates, as piecewise dating was not applicable in profiles with constant or reversed concentrations of excess ^{210}Pb with depth. Deviations from the expected value ranged from 0 to 15% in scenarios D and E (20% to 50% increase in MAR), and were up to 60% in models with a 200% increase in MAR (scenario F). Deviations were of a 10% in a 3-fold increase scenario (G) where CF:CS was applied below the 'disturbed' layer, while deviations from the expected value ranged from 1 to 22% when using the CRS model (Fig. 5). Results were similar for both ecosystem types, seagrasses and mangroves/tidal marshes.

3.2.3 Erosion

We ran three simulations (H, I and J) to represent recent (H) and past erosion events (I and J) (Fig. 3c). Simulations of erosion yielded lower excess ^{210}Pb concentrations than those of the 'ideal' reference profile (type VII, Fig. 2), and excess ^{210}Pb dating horizons were found at shallower depths in these simulations (Fig. 3c). Consequently, excess ^{210}Pb inventories (activity per unit area) in eroded profiles were lower than expected from atmospheric deposition (reference ideal profile A_0: 3900 Bq m^{-2}). Inventories of simulated seagrass sediments had a deficit of 2,450 Bq m^{-2} (60%), 1,250 Bq m^{-2} (30%) and 600 Bq m^{-2} (15%) in erosion scenarios H, I, and J, respectively, while these deficits were of 900 Bq m^{-2} (22%), 700 Bq m^{-2} (19%) and 600 Bq m^{-2} (15%) in mangrove and tidal marsh sediments. As seagrass ecosystems have lower sedimentation rates, a greater proportion of the excess ^{210}Pb inventory was comprised in the top 10 cm of the sediment column and thus eroded. Simulations of past erosion events, which can be identified deeper in the profile, produced breaks in the slope of excess ^{210}Pb concentrations (Fig. 3c) similar to those of type II, yet showing an increase in the slope (Fig. 2). Simulated erosion scenarios did not result in a large impact in MAR and C_{org}-MAR estimated by the CF:CS model under the conditions of this simulation (Fig. 5). The steeper gradient in excess ^{210}Pb concentrations produced by past erosion events resulted in a slight decrease in average MAR. Consequently, derived C_{org}-MAR decreased by only 7% and 2% in seagrass and mangrove habitats, respectively. The magnitude of erosion is better estimated by the deficit in inventories of excess ^{210}Pb, rather than by sedimentation rates. The comparison between sediment records can provide with information about the degree of erosion (Fig. 3c). The C_{org} stocks over the last 100 yr were 20% and 5% lower in seagrass and in mangrove/tidal marsh sediments, respectively, compared to the corresponding 'ideal' profile under non-eroded conditions. Part of this is likely related to the fact that the concentration of C_{org} is not changed, which in reality may actually change since fine sediments, where C_{org} is more efficiently adsorbed, are more easily eroded and OM is remineralized when exposed to oxic conditions during resuspension (Burdige, 2007; Lovelock et al., 2017a; Serrano et al., 2016a) (see simulations 3.2.4 and 3.2.5). Consequently, losses could be significantly larger, as shown in some papers (Macreadie et al., 2013, 2015; Marbà et al., 2015; Serrano et al., 2016a).

3.2.4 Sediment grain size distribution

Coarse sediments are often unsuitable for ^{210}Pb dating as they may lead to very low excess ^{210}Pb concentrations. We simulated excess ^{210}Pb concentration profiles in a coarse sand sediment (scenario K, Fig. 4a). This led to diluted excess ^{210}Pb concentrations where sediments are coarser, and thus, like erosion processes, produced profiles with lower specific activities of excess ^{210}Pb. However, if the ^{210}Pb concentration profiles could be used, coarse but homogeneous grain size distribution with depth did not have any impact in MAR and C_{org}-MAR estimated by the CF:CS model. However, the CRS model underestimated the sedimentation rate by 15% in both habitats (Fig. 5). The shortening of the excess ^{210}Pb horizons overestimates sediment age at bottom layers, due to the omission of a higher fraction of the total integrated excess ^{210}Pb activity from A_m and I at depths where excess ^{210}Pb concentrations are closer to zero. This effect is known as the old-date error of the CRS model and could be corrected as described in Binford, (1990).

Simulations of varying grain size distribution with depth (scenarios L and M, Fig. 4b) led to stepwise excess ^{210}Pb profile forms (type V, Fig. 2). A sharp increase in excess ^{210}Pb concentrations in surface layers can be produced by the presence of finer sediments (scenario L) where ^{210}Pb is preferentially associated, resulting in steeper slopes in excess ^{210}Pb profiles. As a result, sedimentation rates were 10 to 40% lower than those estimated for the ideal profile in seagrass sediments and between 10 to 15% lower in mangrove/tidal marsh sediments (Fig. 5). The higher bound of these ranges correspond to the results of the CRS model, in which excess ^{210}Pb concentrations are inversely related to the sedimentation rate, and thus higher excess ^{210}Pb concentrations result in lower accumulation rates.

When coarser sediments dominate at the surface layers (scenario M), the simulated profiles obtained were similar to those of mixing and accelerated sediment accumulation in recent years (types II, III and IV). On one hand, the dilution of the ^{210}Pb concentrations caused by the deposition of coarse sediments in surface layers was interpreted by the CRS model as an increase in the sedimentation rate, while a flattening of the slope of excess ^{210}Pb concentrations also increased accumulation rates estimated by the CF:CS model. With coarser sediments at surface layers, the CF:CS model overestimated average MAR and C_{org}-MAR by 30% and 10% in seagrass and mangrove sediments, respectively, while the CRS model resulted in only a 6% and 1% overestimation, respectively (Fig. 5). The deposition of coarse sediments may indicate exceptional increases in sedimentation in the case of storm surge deposits or pulsed sediment deliveries. However, the presence of coarse sediments is often related to a reduction in the deposition of fine particles or to the transport and erosion of these in high energy environments, leading to a variation in the excess ^{210}Pb flux onto the sediment surface, considered constant through time by the three classic dating models. Where coarse sediments are deposited on the surfaces, some corrections, such as normalization of excess ^{210}Pb concentrations, are required before the application of any of the ^{210}Pb dating models to obtain reliable estimates of MAR and C_{org}-MAR (see section 4.6).

3.2.5 Organic matter decay

Two different scenarios with low and high sediment organic matter (OM) content (16.5% and 65%, respectively) were modelled related to the OM decay. Variation in OM decay (from a starting level of 16.5%) only slightly affected the excess ^{210}Pb concentration profiles (Fig. 4c). A slight shortening of excess ^{210}Pb profiles due to compaction and subtle higher excess ^{210}Pb concentrations at surface (where OM decay is greater) were the main anomalies observed in modelled ^{210}Pb concentration profiles. These alterations caused an underestimation of actual MAR and C_{org}-MAR of between 10 and 20% in both habitats and by both models, with lower MAR observed when sediments consisted of fast labile OM (experiencing a decay of 0.01 - 0.03 d^{-1}) (Lovelock et al., 2017b). These changes were driven by the lower OM contents, which caused a decrease in the total accumulated mass over time. In contrast, OM decay in very rich organic sediments (65% OM) greatly affected modelled excess ^{210}Pb concentration profiles under any of the rates of decay considered in this simulation (0.00005

d^{-1}, 0.0005 d^{-1} and 0.01 - 0.03 d^{-1}) (Fig. 4d). Increased excess ^{210}Pb concentrations at the surface, reversal of excess ^{210}Pb concentrations (such as in type IV) and significant compaction of excess ^{210}Pb profiles were observed in simulated scenarios Q, R and S. Derived C_{org}-MAR were 50 - 60% lower as estimated by both dating models in both habitats types (Fig. 5). Mass accumulation in vegetated coastal ecosystems is the result of the balance between material accretion (detritus and sediment) from autochthonous and allochthonous sources, decomposition and erosion (e.g. Mateo et al., 1997). The estimates of C_{org}-MAR are the net result of C_{org} accumulation over a centennial time scale as they are based on the C_{org} presently available and not the amount originally deposited. Therefore, the determination of mean C_{org}-MAR will be dependent on the time scale over which they are calculated.

3.2.6 General remarks

Among ecosystems, both the CF:CS and the CRS models were less vulnerable to anomalies in mangrove/tidal marsh compared to seagrass sediments. Higher sedimentation rates lead to deeper excess ^{210}Pb dating horizons and thus the fraction of ^{210}Pb profile affected by anomalies was lower in mangrove/tidal marsh than in seagrass sediments. In particular, anomalies caused by mixing or 2- to 3-fold acceleration in sedimentation had larger effects on the CF:CS derived accumulation rates, while alterations caused by heterogeneous grain size composition primarily affected the CRS derived results (Fig. 5). The decay of OM in very rich organic sediments (> 50% OM) was the process that caused the largest deviations in MAR and C_{org}-MAR in all ecosystems. However, these effects were the result of a decrease in the total accumulated mass over a centennial time scale through OM decay rather than due to anomalies in the excess ^{210}Pb profile. Indeed, this effect could reasonably be ignored in most cases since vegetated coastal ecosystems rarely contain OM concentrations > 25% (Table 1), for which the deviation in computed MAR and C_{org}-MAR was below 20%.

Overall, simulations showed that the variability in MAR and hence C_{org}-MAR due to sedimentary processes and differences in sediment composition was moderately low when appropriate dating models were applied and interpreted. Deviations in the determination of C_{org}-MAR within 20% confirmed that the ^{210}Pb dating technique is secure, especially since in most of the sedimentary processes tested the accumulation rates were underestimated (Fig. 5). However, while these uncertainties might be acceptable for the determination of mean MAR and C_{org}-MAR over a centennial time scale, they may not allow the determination of a detailed geochronology, historical reconstruction, or to ascertain rates of change and fluxes at specific times. In that event, additional tracers or geochemical, ecological and historical data need to be used in concert with ^{210}Pb to validate the ^{210}Pb chronologies in vegetated coastal sediments.

Biogeosciences Discuss., https://doi.org/10.5194/bg-2018-78
Manuscript under review for journal Biogeosciences
Discussion started: 10 April 2018

4 Approaches and Guidelines

Retrieving reliable C_{org}-MAR depends on the correct diagnosis of the intervening sedimentary processes. However, similarities in simulation outcomes and variation associated with anomalies in excess ^{210}Pb profiles point to the need for additional sources of evidence to discriminate between alternative processes and constrain ^{210}Pb-derived estimates.

^{210}Pb results can be combined with geophysical analyses to help in constraining the depositional history of sediments. X-ray radiographies, X-ray fluorescence (XRF), CAT (computerized axial tomography) scans or magnetic susceptibility are non-destructive analyses that can be conducted prior to core processing and subsampling in order to identify changes in the composition of sediments with depth or provide evidence of mixing. For instance, using X-ray radiographs bioturbation is shown as to result in discontinuous physical stratification with active burrows occasionally being preserved (Sun et al., 2017). ^{137}Cs or other independent radioactive tracers can be used to corroborate ^{210}Pb geochronologies. However, in its absence, geochemical information combined with knowledge on events related to land-use and/or environmental changes (e.g. by means of photographic evidence, Swales et al. 2015) can also be used as a tool to validate ^{210}Pb geochronologies and interpret excess ^{210}Pb profiles appropriately. In Table 4 we have summarized the steps to characterize ^{210}Pb profiles and the sedimentary processes most likely involved and suggest several techniques to complement the ^{210}Pb dating method to obtain reliable MAR and C_{org}-MAR.

4.1 Short-lived radionuclides (^{234}Th, ^{228}Th, ^{7}Be): mixing or rapid sedimentation

Tracers such as ^{234}Th, ^{7}Be and ^{228}Th with properties such as particle-reactivity and relatively short half-lives (24.1 days, 53.3 days and 1.9 years, respectively) are suitable to quantify sedimentation processes at scales from several months (^{234}Th and ^{7}Be) to a decade (^{228}Th), and are sensitive indicators of mixing in the zone of constant, scattered or reversed excess ^{210}Pb concentrations (Types II, III, IV, Fig, 2) (Cochran and Masqué, 2005; Sommerfield and Nittrouer, 1999). In addition, demonstrating the presence of an excess of a short-lived radionuclide can give confidence that there is little material missing from the top of the sediment record and no recent erosion. An example is documented by Smoak and Patchineelam (1999), who obtained a ^{210}Pb concentration profile affected by bioturbation in a mangrove ecosystem in Brazil (Box 1).

Mixing, either due to bioturbation or hydrodynamic energy, is the most common process affecting vegetated coastal sediment records. Although the presence of vegetation tends to reduce the depth of sediment mixing (Duarte et al., 2013), the mixed layer can extend to depths of 10-15 cm as is typical for marine sediments globally (Boudreau, 1994). Valid estimates of sedimentation rates (within 15% variability as shown in section 3.2.1) can still be obtained using the dating models described above, however this can only be possible in sediments where excess ^{210}Pb is buried below the mixed layer prior to decay, i.e., the residence time of sediments in the mixed layer must be shorter than the effective dating time scale (~100 yr) (Crusius et al., 2004). In the example from Smoak and Patchineelam (1999) (Box 1), where mixing extends to a depth of 11

Biogeosciences Discuss., https://doi.org/10.5194/bg-2018-78
Manuscript under review for journal Biogeosciences
Discussion started: 10 April 2018

cm, the sedimentation rate had to be ≥1.1 mm yr^{-1} in order for ^{210}Pb to be a useful chronometer (residence time in the mixed layer = 110 mm / 1.1 mm yr^{-1} = 100 yr, which is within the effective dating time scale of ^{210}Pb).

Where mixing is not apparent, constant excess ^{210}Pb concentration profiles might be due to rapid increases of sedimentation. Such (recent) increases in sedimentation rate can be estimated from the slope of the best-fit lines of the plots of ^{7}Be, excess ^{234}Th and ^{228}Th activity against cumulative mass, as Alongi et al. (2005) showed in a mangrove ecosystem in Jiulongjiang Estuary, China (Box 2). However, the use of short-lived radionuclides to derive recent increases in sedimentation rates is restricted to habitats with high accumulation rates (i.e. > 4 mm yr^{-1}, being the last 10 yr comprised in the top 4 cm) due to their relatively short half-lives. Because of its half-life, excess ^{228}Th, might be the only suitable tracer to be used in mangrove/tidal marsh ecosystems where sedimentation rates are on average 5 - 7 mm yr^{-1} (seagrass sedimentation rates average 2 mm yr^{-1}; Duarte et al., 2013). The other short-lived radionuclides might only be applied to assess the magnitude of mixing or recent erosion in vegetated coastal sediments.

4.2 Artificial radionuclides to validate ^{210}Pb geochronologies

Independent validation of the chronology is essential to ensure a high level of confidence in the results (Smith, 2001). True varves used to validate chronologies in lake sediments do not occur in vegetated coastal sedimentary sequences, and thus transient signals such ^{137}Cs or $^{239+240}Pu$ become the most commonly used option to validate ^{210}Pb chronologies (Lynch et al., 1989; Sanders et al., 2010). ^{137}Cs and $^{239+240}Pu$ were delivered globally into the environment through the testing of high-yield thermonuclear weapons in 1950s to early 1960s. ^{137}Cs and $^{239+240}Pu$ are used as chronometers in sediments either by assuming that the peak in activity corresponds to the fallout peak in 1963 or the depth of its first detection corresponds to the onset of fallout in the early 1950. In addition, ^{137}Cs can also display a peak of elevated activity in sediment cores from Europe and the Mediterranean region, corresponding to the emissions caused by the Chernobyl accident in 1986, which can also help to validate ^{210}Pb chronologies (Callaway et al., 1996). These isotopes can also be used as tracers of bioturbation (Crusius et al., 2004) or acceleration of sedimentation during the past 50 years (Appleby, 1998; Cearreta et al., 2002; Lynch et al., 1989; Sharma et al., 1987).

However, the use of ^{137}Cs might have some limitations in vegetated coastal sediments. Two-thirds of the ^{137}Cs activity released due to the tests in the atmosphere decayed after 5 decades, rendering the identification of peaks and its correspondence to the early 50's and 60’s depths more difficult to determine. In addition, the absence of ^{137}Cs signal is reportedly a problem in sediment cores from habitats located in the Southern hemisphere and near the Equator and possibly in seagrass sediments globally, as no studies using ^{137}Cs were found in our literature search. The low ^{137}Cs bomb-test fallout in these regions (Kelley et al., 1999; Ruiz-Fernández and Hillaire-Marcel, 2009), the greater solubility of ^{137}Cs in seawater and the presence of sands, particularly in seagrass sediments (Koch, 2001), are conditions that do not favor the adsorption of ^{137}Cs (He and Walling, 1996a), and may lead to its mobility (Davis et al., 1984), due to its low partition coefficient in seawater ($K_d = 10^2$ to 10^3, Bruland, 1983). This effect could be intensified in the intertidal zone, which is not permanently submerged, due to periodic changes in the water table. These factors together may compromise the use of ^{137}Cs to validate some ^{210}Pb geochronologies and to estimate MAR and C_{org}-MAR in vegetated coastal ecosystems. In contrast, Pu isotopes (^{239}Pu half-life = 24,100 yr and ^{240}Pu half-life = 6,500 yr), although are also dependent on the distribution of bomb-test fallout, would appear to offer several advantages over ^{137}Cs in these environments, as $^{239+240}$Pu is relatively immobile under both freshwater and saltwater conditions (Crusius and Anderson, 1995). For instance, Sanders et al. (2016) determined sedimentation rates and $^{239+240}$Pu penetration depths to study nutrient and C_{org} accumulation in intertidal mangrove mudflats of Moreton Bay, Australia. Nevertheless and because of the limitations to validate older ^{210}Pb dates near the base of the core, and the low inventories of bomb-test fallout in coarse sediments, alternative tracers might need to be used.

4.3 Geochemical information of sediments

Besides the irregular shape of excess ^{210}Pb profiles, the absence of a secondary radioactive tracer to validate ^{210}Pb results can make interpretation even more complicated. However, geochemical information in the sediment column can provide the potential for an additional temporal frame and can also help to explain sedimentary processes that could be misinterpreted (e.g., increasing sedimentation rates, higher primary productivity or reduction of sediment supply). Analyses of additional proxies (pollen, diatom, nutrient concentrations, stable isotopes or trace metal records; López-Merino et al., 2017) that are based on well-described historical events at the study sites (e.g. pollution, crops and land-clearance) could be used in the absence of secondary radioactive tracers to corroborate ^{210}Pb derived dates and accumulation rates. For instance, stable Pb isotopes or total Pb concentrations in sediments are related to the history of use of leaded gasoline in the area and can be used to identify age marks corresponding to peaks in its use or changes in lead sourcing. An example can be found in seagrass sediment cores from Florida Bay, USA (Holmes et al., 2001) or in Gehrels et al. (2005) that combines marsh elevation reconstructions with a precise chronology derived from pollen analysis, stable isotopes, ^{210}Pb and artificial radionuclides (^{206}Pb, ^{207}Pb, ^{137}Cs, ^{241}Am). Additionally, trace metal enrichment factors and carbon and nitrogen isotopic composition of organic matter profiles provide information about environmental changes for which historical information may be well known, i.e., human settlement, onset of touristic industry, temporal evolution of cropland areas or histories of variation in plant communities (Mazarrasa et al., 2017; Ruiz-Fernández and Hillaire-Marcel, 2009; Serrano et al., 2016c).

Changes in the depth distribution of elements consistent with shifts in excess ^{210}Pb concentration profiles might be associated with changes in sedimentation or erosion processes. For instance, instantaneous depositional event layers can be identified in the sedimentary record as isolated minimums of excess ^{210}Pb concentrations (Jaeger and Nittrouer, 2006; Smoak et al., 2013), but also as variations in grain size composition, OM, water content or dry bulk density (Walsh and Nittrouer, 2004) (Box 3). As mentioned previously, changes in sediment mineralogy can be discerned trough X-radiographs, XRF or CAT-scans, but also through other radionuclides, like ^{226}Ra and ^{40}K, the profiles of which can be measured together with those of

^{210}Pb through gamma spectrometry. In particular, ^{40}K is also part of the mineral matrix and is often used as a surrogate for clay content (Garcia-Orellana et al., 2006; Tsabaris et al., 2007; Xu et al., 2015).

4.4 ^{226}Ra concentration profiles

Excess ^{210}Pb concentrations are determined by subtracting supported ^{210}Pb to total ^{210}Pb concentrations assuming it is in equilibrium with ^{226}Ra. ^{226}Ra is most often determined via gamma counting the lower sections of the core (based on the gamma ray energies of its daughters ^{214}Bi and ^{214}Pb, at 609.3 keV and 351.9 keV). Alternatively, supported ^{210}Pb is determined from the region of constant and low ^{210}Pb concentrations at depth, assuming that ^{226}Ra or supported ^{210}Pb are constant throughout the sediment core (Binford, 1990). However, this might not be always the case, especially in heterogeneous profiles consisting of a variety of sediment types or varying clay fractions (Aalto and Nittrouer, 2012) or in records containing episodes of rapid sedimentation (Norton et al., 1992). In addition, equilibrium of ^{210}Pb supported with ^{226}Ra might be compromised in surface sediments where ^{222}Rn is deficient (Appleby, 2001). Although variations in ^{226}Ra activity with depth are small in most cases, accurate determination of ^{226}Ra might be crucial in sediments with low total ^{210}Pb concentrations (e.g., due to the presence of coarse sediments or low ^{210}Pb atmospheric fallout), where slight variations in the supported ^{210}Pb may result in significant errors in the estimation of excess ^{210}Pb concentrations (Box 4). To avoid deviations in excess ^{210}Pb concentration profiles associated with variations in supported ^{210}Pb, it is recommended to measure ^{226}Ra concentration profiles and use depth-specific values to estimate excess ^{210}Pb. Besides, profiles of ^{226}Ra might serve to discriminate between intense mixing or erosion (or negligible net modern accumulation) processes, since in the former case there would be excess ^{210}Pb, while it will be absent in the later.

4.5 Excess ^{210}Pb inventories (*I*) to estimate sediment erosion

Assessing the extent of erosion requires the study of the excess ^{210}Pb inventories. The total deficit of excess ^{210}Pb inventory per unit area for a given location can be compared with the equivalent inventory of a nearby non-eroded reference site. This approach has been widely used in terrestrial soils (Martz and Jong, 1991; Walling et al., 2003) and has been recently successfully applied to assess erosion of seagrass sediments (Greiner et al., 2013; Marbà et al., 2015; Serrano et al. 2016b) (Box 5).

4.6 Normalization of excess ^{210}Pb concentrations and sieving of sediments

Dating models assume rapid and non-discriminatory removal of radionuclides from the water column regardless of major changes in grain size or OM content along a sediment record. Radionuclide adsorption onto sediments is strongly governed by the binding capacity of the settling particles (Cremers et al., 1988; Loring, 1991), thus its scavenging is enhanced by fine-grained texture (He and Walling, 1996) and OM particulates (Nathwani and Phillips, 1979; Yeager and Santschi, 2003). Variations in the influx of these particles into vegetated coastal sediments may proportionally affect the influx of particle bound excess ^{210}Pb (as long as it is still available), thus violating the assumption of constant flux of the CRS model and leading to subsections and irregularities of excess ^{210}Pb profiles. Constant or reversed patterns in excess ^{210}Pb concentrations, which could be easily mistaken for reworked deposition, could be caused, for instance, by vertical fluctuations of grain size due to seasonal variations of sediment discharge or reoccurring tidal currents. Sediment studies often attempt to minimize these effects by normalizing radionuclide concentrations to granulometric or geochemical parameters that reduce the influence of preferential adsorption by fine sediments and OM (Álvarez-Iglesias et al., 2007; Loring, 1991; Wan et al., 2005), allowing to obtain excess ^{210}Pb concentration profiles showing an exponential decreasing trend with depth (Kirchner and Ehlers, 1998; Sun et al., 2017). Radiometric applications in coastal sediments have traditionally opted for grain size normalizers such as the < 4 µm, < 63 µm fraction or Al content (Álvarez-Iglesias et al., 2007; Sanders et al., 2010; Sun et al., 2017; Walsh and Nittrouer, 2004), while in dynamic, sandy-rich coastal systems where the mud fraction is small, normalization by OM content has been shown to be more effective (Van Eaton et al., 2010). Equation 4 can be used to normalize excess ^{210}Pb concentrations ($^{210}Pb_{xs\text{-}NORM}$ in Bq kg^{-1}) by grain size fractions, OM content or other geochemical parameters that control the variation of the input of excess ^{210}Pb and play an important role in the distribution of initial excess ^{210}Pb concentrations.

$$^{210}Pb_{xs\text{-}NORM} = {}^{210}Pb_{xs\text{-}MEAS}(NP_{AVG}/NP_m) \qquad (Eq.\ 4)$$

where $^{210}Pb_{xs\text{-}MEAS}$ is the measured activity at depth *m*, and (NP_{AVG}/NP_m) is the ratio of the core average normalizing parameter to the content of the normalizing parameter of sediment at depth *m*. For instance, multiplication by this ratio corrects measured ^{210}Pb activities for variations in OM with respect to an average core value.

Reliable sedimentation histories are difficult to obtain in vegetated coastal sediments consisting of coarse particles or coarse-grained carbonates where excess ^{210}Pb is less efficiently adsorbed (Wan et al., 1993). In such situations, the analysis of ^{210}Pb in the smaller sediment fraction (i.e. < 63µm or < 125 µm) is recommended in order to concentrate ^{210}Pb and reduce the dilution effect caused by coarse sediment fractions. This methodology has been applied in mangrove ecosystems from arid regions (Almahasheer et al., 2017) where excess ^{210}Pb flux is very low, and carbonate-rich seagrass sediments (Holmes et al., 2001).

4.7 Maximum penetration depth of excess ^{210}Pb

A detailed chronology cannot be estimated if mixing affects the whole or the vast majority of the sediment record. However, information such as the total historical inventory of elements, like nutrients accumulated at a site, and the maximum conservative sedimentation rate can still be estimated. The penetration-depth method (Goodbred and Kuehl, 1998; Jaeger et al., 2009) uses the maximum penetration depth of excess ^{210}Pb (depth of disappearance) as a marker horizon for sediments that are ~100 yr old. By locating the 100 yr horizon, independently of subsequent alteration of sedimentary processes and of assumptions of the CF:CS or CRS models, an upper estimate of the centennial average sedimentation rate can be derived. It is important to highlight that by using this method, the rates of change or fluxes cannot be estimated and these types of excess ^{210}Pb profiles may be of little use in establishing accurate chronostratigraphies.

5 Conclusions

^{210}Pb serves as a tool to establish recent (last ~100 years) MAR and C_{org}-MAR in vegetated coastal ecosystems. ^{210}Pb dating techniques provides crucial information for the study of sediment accretion and carbon sequestration, the latter being its principal use in Blue carbon science. Indeed, also can provide accurate geochronologies for the reconstruction of environmental processes based on the study of the sedimentary sequences found underneath coastal vegetated ecosystems. However, ^{210}Pb reconstruction studies may be difficult to conduct in many of the sediments from mangrove, tidal marsh and seagrass ecosystems, where unaltered sedimentary records are rare. Shallow vegetated coastal sediments are often composed by heterogeneous sediments and may be disturbed by natural and anthropogenic processes (i.e., mixing through wind and tidal currents, bioturbation by benthic fauna, acceleration of sedimentation or erosion due to clearing of the catchment areas and rivers impoundment). These factors may lead to anomalies in the ^{210}Pb concentration profiles from those expected, that combined with the limitations associated with the use of secondary tracers can constrain the derived age models and their interpretation. This is particularly challenging in seagrass sediments because of their relatively low sedimentation rates and high sand content where ^{210}Pb is less efficiently adsorbed.

The sensitivity of estimated MAR and C_{org}-MAR to the various processes that can alter the ^{210}Pb concentration profiles can be assessed, however complementary analyses are also required to identify the potential processes involved. In particular, radiotracers such as ^{137}Cs, $^{239+240}$Pu, ^{228}Th, ^{234}Th, ^{7}Be and ^{226}Ra may help refine the estimates of sedimentation and mixing rates and the identification of the occurrence of erosion obtained from excess ^{210}Pb profiles. However, in their absence, the distribution of physical and geochemical parameters with depth such as sediment grain size, DBD, OM content, stable isotopes or trace metals could be used to support ^{210}Pb results. Indeed, normalization by grain size, OM and/or lithogenic metal concentrations (e.g. Al) may contribute to minimize potential impacts related to differential scavenging of ^{210}Pb and render usable ^{210}Pb concentration profiles, while obtaining additional information on the presence of textural and chemical stratigraphy. While attention should be paid to the limitations of ^{210}Pb-derived chronologies in vegetated coastal ecosystems, the guidelines provided here should help to understand the limitations that arise from anomalous ^{210}Pb profiles retrieved from vegetated coastal sediments and to develop a strategy to strengthen the evaluation of MAR and C_{org}-MAR.

Biogeosciences Discuss., https://doi.org/10.5194/bg-2018-78
Manuscript under review for journal Biogeosciences
Discussion started: 10 April 2018

Appendix A: Simulation methods

Mixing

To simulate mixing, we estimated the accumulated excess ^{210}Pb activity per unit area over the top 5 cm of the ideal excess ^{210}Pb profile (I_{5cm}: 2126 Bq m^{-2} in seagrass, and I_{5cm}: 723 Bq m^{-2} in mangrove/tidal marsh sediments) (Supplementary, table 1). We split this inventory within the 5 upper centimetres using a random function, the outputs of which fell within the standard deviation (±SD) of the mean of the excess ^{210}Pb activity in these sections (±107 Bq m^{-2} in seagrass; and ±9 Bq m^{-2} in mangrove/tidal marsh sediments). We run the simulation several times until we obtained three scenarios (A, B, C) of mixing encompassing a range of surface mixed layers (SML) (Supplementary, Tables 2a and 2b). Mixing A (k_m: ∞ g^2 cm^{-4} yr^{-1}) consisted of constant excess ^{210}Pb concentrations with depth in surface layers; mixing B (k_m: 20 - 23 g^2 cm^{-4} yr^{-1}) was characterised by a decrease in the slope of excess ^{210}Pb concentrations in top layers; and mixing C represented deep mixing from 5 cm to 10 cm (k_m: 7 - 10 g^2 cm^{-4} yr^{-1}). Excess ^{210}Pb concentrations per unit area (A) were converted to excess ^{210}Pb concentrations (C) in Bq kg^{-1}, which we averaged every two layers to represent smooth transitions. Sedimentation and derived C_{org}-MAR were estimated from the modelled profiles using the CF:CS and the CRS models. The CF:CS model was applied below the depth of the visually apparent SML (3 cm) in scenarios A and B to avoid overestimation of MAR. In the case of the CRS model, ages were determined at each layer and average centennial MAR was estimated by dividing the cumulative mass (g cm^{-2}) over the last 100 yr by its age (i.e., 100 yr).

Increasing sedimentation

We simulated an enhancement of the mass accumulation rate that could result, for instance, from increased sediment run-off due to coastal development, by increasing the basal MAR (0.2 g cm^{-2} yr^{-1} and 0.3 g cm^{-2} yr^{-1} in seagrass and mangrove/tidal marsh, respectively) by different magnitudes (20%, 50%, 200% and 300%). Increases in MAR were simulated over the top 6 cm and 23 cm of the idealized excess ^{210}Pb concentration profile, which represent the last 30 years of accumulation in seagrass and mangrove/tidal marsh sediments, respectively. Last century mass accumulation rates expected at ideal profiles were estimated through the weighted average of MAR at each sediment layer, weights being the time elapsed between layers (Supplementary Tables 3a and 3b). Excess ^{210}Pb concentrations *(C_m)* as a result of increased MAR were estimated through equation A1 at each layer. Simulations of increasing MAR generated four profiles per habitat type (scenarios D, E, F and G) (Fig. 3b). Average MAR and C_{org}-MAR were estimated from the modelled profiles using the CF:CS and CRS models. The CF:CS model was applied piecewise in scenarios D, E and F, and below reversed excess ^{210}Pb concentrations in top layers in scenario G.

$$C_m = \frac{\lambda \cdot I_m}{MAR \cdot 10} \tag{A1}$$

where λ is the decay constant of ^{210}Pb (0.0311 yr^{-1}) and I_m is the excess ^{210}Pb inventory accumulated at layer m. 10 allows unit conversion to Bq kg^{-1}.

Erosion

Erosion in vegetated coastal sediments can occur due to high-energy events (Short et al., 1996), vegetation loss and subsequent destabilization of sediments (Marbà et al., 2015) or mechanical disturbances (e.g. Serrano et al., 2016c). We ran three simulations to represent recent (H) and past erosion events (I and J) (Fig. 3c). We started with an ideal excess ^{210}Pb profile with a total initial excess ^{210}Pb inventory of 3,900 Bq m^{-2}, thereon, to simulate erosion we removed the excess ^{210}Pb inventory accumulated in the top 0 - 5 cm (H), middle 5 – 10 cm (I) and 10 – 15 cm sections (J) in sediments from both habitat types (mangrove/tidal marsh and seagrass). Resulting excess ^{210}Pb activity per unit area (Bq m^{-2}) were converted to excess ^{210}Pb concentrations (Bq kg^{-1}) by dividing by the corresponding mass depth (g cm^{-2}) at each section after correcting the latter for the loss of sediment layers (Supplementary, Tables 4a and 4b). ^{210}Pb concentrations were averaged every two layers to simulate smooth transitions rather than a sharp discontinuity after and erosion event. We estimated the resulting average MAR and C_{org}-MAR using the CF:CS model (applied piecewise in erosion scenarios I and J). The CRS model could not be applied, since the overall core inventory *(I)* was incomplete.

Changes in sediment grain size

We simulated various excess ^{210}Pb concentration profiles with changes in sediment grain size distribution using the approach described by He & Walling (1996), where the specific surface area of particles exerts a primary control on the excess ^{210}Pb concentrations adsorbed:

$$C\ (S_{sp}) = \mu \cdot S_{sp}^{0.67} \qquad \text{(Eq. A2)}$$

where C is excess ^{210}Pb concentration (mBq g^{-1}), S_{sp} is the specific surface area of the sediment particles (m^2 g^{-1}), and μ is a constant scaling factor depending upon the initial excess ^{210}Pb activity per unit area (mBq m^{-2}). The excess ^{210}Pb concentration in bulk sediments can also be represented by equation A2 replacing S_{sp} by the mean specific surface area S_{mean} (m^2 g^{-1}) of the bulk sample. In this work, we estimated μ at each layer of an ideal excess ^{210}Pb profile in seagrass and mangrove/tidal marsh sediments if ideally the S_{sp} throughout the core is 0.07 m^2 g^{-1}, corresponding to a mean particle size of 63 μm. The surface area can be estimated as (Jury and Horton, 2004):

$$S_{sp} = \frac{3}{\rho \cdot r} \qquad \text{(Eq. A3)}$$

where ρ is the density of the sediment particles and r is the mean radius of sediment particles, which are considered spherical.

We estimated the weighted mean specific surface area of a very coarse sediment composed of 70% coarse sand (500 – 1000 μm) and 30% medium sand (250 – 500 μm) (S_{mean} = 0.007 m^2 g^{-1}), through equation A3 (size scale: Wentworth, 1922). Bulk density (ρ) of sediment fractions was considered: 1.6 g cm^{-3} for medium sand and 1.8 g cm^{-3} for coarse sand. Then, we simulated excess ^{210}Pb concentration profiles as a function of the specific surface area applying equation A2 to an ideal excess ^{210}Pb concentration profile (scenario K) (Supplementary, Tables 5a and 5b). Additionally, we simulated a shift from

Biogeosciences Discuss., https://doi.org/10.5194/bg-2018-78
Manuscript under review for journal Biogeosciences
Discussion started: 10 April 2018

medium sands (coarse) to clay (fine) sediments and *vice versa*, as could result, after the restoration or loss of vegetated coastal ecosystems. The percentage of sands along the core was changed using a random function (from 60 ± 20% to 15 ± 5% and *vice versa;* scenarios L and M) (Supplementary, Tables 6a and 6b). The shift was simulated at the same age depth (30 yr before collection) in all scenarios and habitat types. The mass depth term was corrected in each case for changes in grain size, which lead to variations in DBD with depth. Bulk density (ρ) of sediment fractions was considered: 0.4 g cm^{-3} for clays and 1.6 g cm^{-3} for medium sands. In addition, the value of μ was readjusted at each sediment depth of the ideal profile to represent non-monotonic variations in cumulative dry mass. Excess ^{210}Pb concentration profiles were estimated as a function of the specific surface area that was estimated at each layer according to the various proportions of clay and sand. The average MAR and C_{org}-MAR were estimated using the CF:CS and CRS models. The CF:CS model was applied piecewise in simulated scenarios L and M.

Organic matter decay

Excess ^{210}Pb in vegetated coastal sediments is deposited in association with mineral particles but also with organic particulates (Krishnaswamy et al., 1971; Yeager and Santschi, 2003). Once buried, sediment organic matter (OM) content usually decays with sediment depth and aging due to remineralization of labile fractions, leading to an enrichment of excess ^{210}Pb concentrations. We simulated the resultant excess ^{210}Pb concentration profiles derived from this process in two sediments with different OM contents (16.5% and 65%). The first value (16.5% OM) is within the usual range of tidal marsh, mangrove and in the high range for seagrass sediments (Fourqurean et al., 2012) (Table 1). The second value (65% OM) represents an extreme scenario based in existing studies in seagrass and mangrove ecosystems (Callaway et al., 1997; Serrano et al., 2012). The simulations were run under three OM decay constants assuming: (1) the whole pool of OM is refractory, decaying at a rate of 0.00005 d^{-1} in seagrass and in mangrove/tidal marsh sediments (Lovelock et al., 2017b); (2) 50% of the refractory pool is exposed to oxic conditions, decaying at a rate of 0.0005 d^{-1} in mangrove/tidal marsh sediments; and (3) 50% of the OM pool is labile, decaying fast, although exposed to anoxic conditions, at 0.01 d^{-1} and 0.03 d^{-1} in seagrass and mangrove/tidal marsh sediments, respectively (Lovelock et al., 2017b).

The ^{210}Pb enrichment factor (η) can be determined for a given time after deposition as:

$$\eta(t) = \frac{\chi_s + \chi_{org} \cdot e^{-k_{org} \cdot t}}{\chi_s + \chi_{org}} \qquad \text{(Eq. A4)}$$

where χ_s is the mineral fraction of sediments, χ_{org} is the organic fraction of sediments at time 0, and k_{org} is the decay constant of the OM in sediments. *t* is time and can be estimated as ${}^{m}/_{MAR}$. As time (*t*) increases the exponential term tends to zero, hence the OM stored in the sediment reaches a constant value, where it is no longer decomposed. We assume that the remineralized OM leaves the sediment as CO_2, but in fact a fraction (*f*) would transform to mineral matter as $\chi_s(t) = \chi_{s(0)} + f \cdot \chi_{org(0)} \cdot (1 - e^{-k_{org} \cdot t})$. In our simulations *f = 0* was assumed.

Then, the excess ^{210}Pb concentration of a sample of age *t* with initial concentration C_0 is:

$$C_t = \frac{C_0 \cdot e^{-\lambda t}}{\eta(t)} \tag{Eq. A5}$$

and the total mass accumulated with depth (*M*) above a layer of age *t* is:

$$M = MAR \cdot \chi_S \cdot t + MAR \cdot \chi_{org} \cdot e^{-k_{org} \cdot t} \cdot t \tag{Eq. A6}$$

MAR was estimated using the CF:CS and CRS models and C_{org}-MAR through eq. 3. Organic matter (%OM) in mangrove/tidal marsh sediments was transformed to $\%C_{org}$ using equation A7 (Kauffman and Donato, 2012). In seagrass sediments we applied the relationship reported by Fourqurean et al. (2012) (Eq. A8) (Supplementary, Table 7a and 7b).

$$\%C_{org} = 0.415\ \%OM + 2.89 \tag{Eq. A7}$$

$$\%C_{org} = 0.43\ \%OM - 0.33 \tag{Eq. A8}$$

Competing Interest

The authors declare that they have no conflict of interest.

Author Contribution

A. Arias-Ortiz contributed to the design, data acquisition, analysis, interpretation and wrote the first draft of the manuscript. All authors contributed to the design and data acquisition and/or interpretation, and provided critical review of the manuscript. All authors have read and approved the final version of the manuscript.

Acknowledgements

This work was funded by the CSIRO Flagship Marine & Coastal Carbon Biogeochemical Cluster (Coastal Carbon Cluster), the Spanish Ministry of Economy and Competitiveness (Project EstresX, CTM2012- 32603), the Generalitat de Catalunya (MERS 2014 SGR – 1356), the Edith Cowan University Faculty Research Grant Scheme and King Abdullah University of Science and Technology (KAUST) through baseline funding to CMD. This work contributes to the ICTA 'Unit of Excellence' (MinECo, MDM2015-0552). AAO was funded by a PhD grant from Obra Social "laCaixa". OS was supported by an ARC DECRA (DE170101524). IM was funded by a post-doctoral grant (Juan de la Cierva-Formación) from the Spanish Ministry of Economy, Industry and Competitiveness.

References

Aalto, R. and Nittrouer, C.: ^{210}Pb geochronology of flood events in large tropical river systems, Philos. Trans. R. Soc. A Math. Phys. Eng. Sci., 370, 2040–2074, doi:10.1098/rsta.2011.0607, 2012.

Abril, J. M.: A new theoretical treatment of compaction and the advective-diffusive processes in sediments: a reviewed basis for radiometric dating models, J. Paleolimnol., 30, 363–370, 2003.

Abril, J. M.: A ^{210}Pb-based chronological model for recent sediments with random entries of mass and activities: Model development, J. Environ. Radioact., 151, 64–74, doi:10.1016/j.jenvrad.2015.09.018, 2016.

Abril, J. M. and Gharbi, F.: Radiometric dating of recent sediments: Beyond the boundary conditions, J. Paleolimnol., 48, 449–460, doi:10.1007/s10933-012-9622-5, 2012.

Abril, J. M., García-León, M., García-Tenorio, R., Sánchez, C. I. and El-Daoushy, F.: Dating of marine sediments by an incomplete mixing model, J. Environ. Radioact., 15(2), 135–151, doi:10.1016/0265-931X(91)90048-K, 1992.

Almahasheer, H., Serrano, O., Duarte, C. M., Arias-Ortiz, A., Masque, P. and Irigoien, X.: Low Carbon sink capacity of Red Sea mangroves, Sci. Rep., 7(1), 9700, doi:10.1038/s41598-017-10424-9, 2017.

Alongi, D. M., Sasekumar, A., Chong, V. C., Pfitzner, J., Trott, L. A., Tirendi, F., Dixon, P. and Brunskill, G. J.: Sediment accumulation and organic material flux in a managed mangrove ecosystem: Estimates of land-ocean-atmosphere exchange in peninsular Malaysia, Mar. Geol., 208(2–4), 383–402, doi:10.1016/j.margeo.2004.04.016, 2004.

Alongi, D. M., Pfitzner, J., Trott, L. a., Tirendi, F., Dixon, P. and Klumpp, D. W.: Rapid sediment accumulation and microbial mineralization in forests of the mangrove Kandelia candel in the Jiulongjiang Estuary, China, Estuar. Coast. Shelf Sci., 63, 605–618, doi:10.1016/j.ecss.2005.01.004, 2005.

Alongi, D. M., Trott, L. a., Rachmansyah, Tirendi, F., McKinnon, a. D. and Undu, M. C.: Growth and development of mangrove forests overlying smothered coral reefs, Sulawesi and Sumatra, Indonesia, Mar. Ecol. Prog. Ser., 370, 97–109, doi:10.3354/meps07661, 2008.

Álvarez-Iglesias, P., Quintana, B., Rubio, B. and Pérez-Arlucea, M.: Sedimentation rates and trace metal input history in intertidal sediments from San Simón Bay (Ría de Vigo, NW Spain) derived from ^{210}Pb and ^{137}Cs chronology, J. Environ. Radioact., 98, 229–250, doi:10.1016/j.jenvrad.2007.05.001, 2007.

Appleby, P.: Chronostratigraphic Techniques in Recent Sediments, in Tracking Environmental Change Using Lake Sediments, 1, 171–203, Springer Netherlands., 2001.

Appleby, P. G.: Dating recent sediments by ^{210}Pb : problems and solutions, In Proceedings of a seminar, Helsinki, 2(4), 7–24, 1998.

Appleby, P. G. and Oldfield, F.: The calculation of lead-210 dates assuming a constant rate of supply of unsupported ^{210}Pb to the sediment, CATENA, 5(1), 1–8, doi:10.1016/S0341-8162(78)80002-2, 1978.

Baskaran, M., Nix, J., Kuyper, C. and Karunakara, N.: Problems with the dating of sediment core using excess ^{210}Pb in a freshwater system impacted by large scale watershed changes, J. Environ. Radioact., 138, 355–363, doi:10.1016/j.jenvrad.2014.07.006, 2014.

Bellucci, L. G., Frignani, M., Cochran, J. K., Albertazzi, S., Zaggia, L., Cecconi, G. and Hopkins, H.: ^{210}Pb and ^{137}Cs as chronometers for salt marsh accretion in the Venice Lagoon - links to flooding frequency and climate change, J. Environ. Radioact., 97(2–3), 85–102, doi:10.1016/j.jenvrad.2007.03.005, 2007.

Binford, M. W.: Calculation and uncertainty analysis of ^{210}Pb dates for PIRLA project lake sediment cores, J. Paleolimnol., 3, 253–267, 1990.

Botwe, B. O., Abril, J. M., Schirone, A., Barsanti, M., Delbono, I., Delfanti, R., Nyarko, E. and Lens, P. N. L.: Settling fluxes and sediment accumulation rates by the combined use of sediment traps and sediment cores in Tema Harbour (Ghana), Sci. Total Environ., 609, 1114–1125, doi:10.1016/j.scitotenv.2017.07.139, 2017.

Breithaupt, J. L., Smoak, J. M., Smith, T. J., Sanders, C. J. and Hoare, A.: Organic carbon burial rates in mangrove sediments: Strengthening the global budget, Global Biogeochem. Cycles, 26(3), doi:10.1029/2012GB004375, 2012.

Bruland, K. .: Trace elements in seawater., In *Chemical oceanography*, vol. 1, edited by J. P. Riley and G. Skirrow, London Academic Press, London, pp. 415–496, 1983.

Burdige, D. J.: Preservation of Organic Matter in Marine Sediments: Controls, Mechanisms, and an Imbalance in Sediment Organic Carbon Budgets?, Chem. Rev., 107(2), 467–485, doi:10.1021/CR050347Q, 2007.

Callaway, J., DeLaune, R. and Jr, W. P.: Sediment accretion rates from four coastal wetlands along the Gulf of Mexico, J. Coast. Res., 13, 181–191, 1997.

Callaway, J. C., DeLaune, R. D. and Patrick, W. H.: Chernobyl ^{137}Cs used to determine sediment accretion rates at selected northern European coastal wetlands, Limnol. Oceanogr., 41(3), 444–450, doi:10.4319/lo.1996.41.3.0444, 1996.

Carroll, J. and Lerche, I.: Sedimentary processes : quantification using radionuclides, Elsevier, Oxford, 272, 2003.

Castañeda-Moya, E., Twilley, R. and Rivera-Monroy, V.: Sediment and nutrient deposition associated with Hurricane Wilma in mangroves of the Florida Coastal Everglades, Estuaries and Coasts, 33, 45–58, doi:10.1007/s12237-009-9242-0, 2010.

Cearreta, A., Irabien, M. J., Ulibarri, I., Yusta, I., Croudace, I. W. and Cundy, A. B.: Recent Salt Marsh Development and Natural Regeneration of Reclaimed Areas in the Plentzia Estuary , N . Spain, Estuar. Coast. Shelf Sci., 54, 863–886, doi:10.1006/ecss.2001.0862, 2002.

Chanton, J. P., Martens, C. S. and Kipphut, G. W.: Lead-210 sediment geochronology in a changing coastal environment, Geochim Cosmo Acta, 47(15), 1791–1804, doi:10.1016/0016-7037(83)90027-3, 1983.

Chen, R. and Twilley, R. R.: A simulation model of organic matter and nutrient accumulation in mangrove wetland soils, Biogeochemistry, 44, 93–118, doi:10.1007/BF00993000, 1999.

Chmura, G. L., Anisfeld, S. C., Cahoon, D. R. and Lynch, J. C.: Global carbon sequestration in tidal, saline wetland soils, Global Biogeochem. Cycles, 17(4), 1111, doi:10.1029/2002GB001917, 2003.

Church, T. M., Lord, C. J. and Somayajulu, B. L. K.: Uranium, thorium and lead nuclides in a Delaware salt marsh sediment, Estuar. Coast. Shelf Sci., 13, 267–275, doi:10.1016/S0302-3524(81)80025-4, 1981.

Cochran, J. and Masqué, P.: Natural radionuclides applied to coastal zone processes, Mar. Radioact., 6, 1–21, doi:https://doi.org/10.1016/S1569-4860(05)80002-6, 2005.

Cochran, J. K., Hirschberg, D. J., Wang, J. and Dere, C.: Atmospheric Deposition of Metals to Coastal Waters (Long Island Sound, New York U.S.A.): Evidence from Saltmarsh Deposits, Estuarine, Coast. Shelf Sci. 46, 503-522, doi:10.1006/ecss.1997.0299, 1998.

Craft, C.: Freshwater input structures soil properties, vertical accretion, and nutrient accumulation of Georgia and U.S tidal marshes, Limnol. Oceanogr., 52(3), 1220–1230, doi:10.4319/lo.2007.52.3.1220, 2007.

Cremers, A., Elsen, A., Preter, P. De and Maes, A.: Quantitative analysis of radiocaesium retention in soils, Nature, 335(6187), 247–249, doi:10.1038/335247a0, 1988.

Crusius, J. and Anderson, R. F.: Evaluating the mobility of ^{137}Cs, $^{239+240}$Pu and ^{210}Pb from their distributions in laminated lake sediments, J. Paleolimnol., 13, 119–141, doi:10.1007/BF00678102, 1995.

Crusius, J., Bothner, M. H. and Sommerfield, C. K.: Bioturbation depths, rates and processes in Massachusetts Bay sediments inferred from modeling of ^{210}Pb and $^{239+240}$Pu profiles, Estuar. Coast. Shelf Sci., 61(4), 643–655, doi:10.1016/j.ecss.2004.07.005, 2004.

Cundy, A. B. and Croudace, I. W.: Physical and chemical associations of radionuclides and trace metals in estuarine sediments: an example from Poole Harbour, Southern England, J. Environ. Radioact., 29(3), 191–211, doi:10.1016/0265-931X(95)00031-5, 1995.

Davis, R., Hess, C. and Norton, S.: 137 Cs and 210 Pb dating of sediments from soft-water lakes in New England (USA) and Scandinavia, a failure of 137 Cs dating, Chem. Geol., 44, 151–185, 1984.

Donato, D. C., Kauffman, J. B., Murdiyarso, D., Kurnianto, S. and Stidham, M.: Mangroves among the most carbon-rich forests in the tropics, Nat. Geosci., 4(4), 1–5, doi:10.1038/ngeo1123, 2011.

Du, J. Z., Zhang, J. and Baskaran, M.: Applications of Short-Lived Radionuclides (^{7}Be, ^{210}Pb, ^{210}Po, ^{137}Cs and ^{234}Th) to Trace the Sources, Transport Pathways and Deposition of Particles/Sediments in Rivers, Estuaries and Coasts, in Handbook of Environmental Isotope Geochemistry, Springer, Berlin Heidelberg., 305–329, 2012.

Duarte, C. M.: Global change and the future ocean: a grand challenge for marine sciences, Front. Mar. Sci., 1, 63, doi:10.3389/fmars.2014.00063, 2014.

Duarte, C. M., Losada, I. J., Hendriks, I. E., Mazarrasa, I. and Marbà, N.: The role of coastal plant communities for climate change mitigation and adaptation, Nat. Clim. Chang., 3(11), 961–968, doi:10.1038/nclimate1970, 2013.

Van Eaton, A. R., Zimmerman, A. R., Jaeger, J. M., Brenner, M., Kenney, W. F. and Schmid, J. R.: A novel application of radionuclides for dating sediment cores from sandy, anthropogenically disturbed estuaries, Mar. Freshw. Res., 61(11), 1268–1277, doi:10.1071/MF10028, 2010.

Ember, L., Williams, D. and Morris, J.: Processes that influence carbon isotope variations in salt marsh sediments, Mar. Ecol. Prog. se, 36, 33–42, 1987.

Fonseca, M. S. and Fisher, J. S.: A comparison of canopy friction and sediment movement between four species of seagrass with reference to their ecology and restoration, Mar. Ecol. Prog. Ser., 29, 15–22, doi:10.2307/24817530, 1986.

Fourqurean, J. W., Duarte, C. M., Kennedy, H., Marbà, N., Holmer, M., Mateo, M. A., Apostolaki, E. T., Kendrick, G. A., Krause-Jensen, D., McGlathery, K. J. and Serrano, O.: Seagrass ecosystems as a globally significant carbon stock, Nat. Geosci., 5(7), 505–509, doi:10.1038/ngeo1477, 2012.

Garcia-Orellana, J., Gràcia, E., Vizcaino, A., Masqué, P., Olid, C., Martínez-Ruiz, F., Piñero, E., Sanchez-Cabeza, J. A. and Dañobeitia, J.: Identifying instrumental and historical earthquake records in the SW Iberian margin 210Pb turbidite chronology, Geophys. Res. Lett., 33(24), 1–6, doi:10.1029/2006GL028417, 2006.

Gardner, L. R., Sharma, P. and Moore, W. S.: A Regeneration Model for the Effect of Bioturbation by Fiddler Crabs on ^{210}Pb Profiles in Salt Marsh Sediments, 5, 25–36, 1987.

Gehrels, W. R., Kirby, J. R., Prokoph, A., Newnham, R. M., Achterberg, E. P., Evans, H., Black, S. and Scott, D. B.: Onset of recent rapid sea-level rise in the western Atlantic Ocean, Quat. Sci. Rev., 24(18–19), 2083–2100, doi:10.1016/j.quascirev.2004.11.016, 2005.

Goldberg, E. D., Gamble, E., Griffin, J. J. and Koide, M.: Pollution history of Narragansett Bay as recorded in its sediments, Estuar. Coast. Mar. Sci., 5(4), 549–561, doi:10.1016/0302-3524(77)90101-3, 1977.

Goodbred, S. L. and Kuehl, S. A.: Floodplain processes in the Bengal Basin and the storage of Ganges–Brahmaputra river sediment: an accretion study using ^{137}Cs and ^{210}Pb geochronology, Sediment. Geol., 121(3–4), 239–258, doi:10.1016/S0037-0738(98)00082-7, 1998.

Greiner, J. T., McGlathery, K. J., Gunnell, J. and McKee, B. A.: Seagrass Restoration Enhances "Blue Carbon" Sequestration in Coastal Waters, PLoS One, 8(8), 2013.

Haslett, S., Cundy, A., Davies, C. and Powell, E.: Salt marsh sedimentation over the past c. 120 years along the west Cotentin coast of Normandy (France): relationship to sea-level rise and sediment supply, J. Coast. Res., 19, 609–620, 2003.

Hatton, R., DeLaune, R. and Jr, W. P.: Sedimentation, accretion, and subsidence in marshes of Barataria Basin, Louisiana, Limnol. Oceanogr., 28(3), 494–502, 1983.

He, Q. and Walling, D. E.: Interpreting Particle Size Effects in the Adsorption of ^{137}Cs and Unsupported ^{210}Pb by Mineral Soils and Sediments, J. Environ. Radioact., 30(2), 117–137, 1996a.

He, Q. and Walling, D. E.: Use of fallout Pb-210 measurements to investigate longer-term rates and patterns of overbank sediment deposition on the floodplains of lowland rivers, Earth Surf. Process. Landforms, 21(2), 141–154, 1996b.

Holmes, C. W., Robbins, J., Halley, R., Bothner, M., Brink, M. Ten and Marot, M.: Sediment dynamics of Florida Bay mud banks on decadal time scale, Bull. Am. Paleontol., 361, 31–40, 2001.

Howard, J., Hoyt, S., Isensee, K., Pidgeon, E. and Telszewski, M.: Coastal Blue Carbon: Methods for Assessing Carbon Stocks and Emissions Factors in Mangroves, Tidal Salt Marshes, and Seagrass Meadows, Conserv. Int. Intergov. Oceanogr. Comm. UNESCO, Int. Union Conserv. Nature. Arlington, Virginia, USA., 1–180, 2014.

Howard, J., Sutton-Grier, A., Herr, D., Kleypas, J., Landis, E., Mcleod, E., Pidgeon, E. and Simpson, S.: Clarifying the role of coastal and marine systems in climate mitigation, Front. Ecol. Environ., 15(1), 42–50, doi:10.1002/fee.1451, 2017.

Jaeger, J., Mehta, A., Faas, R. and Grella, M.: Anthropogenic impacts on sedimentary sources and processes in a small urbanized subtropical estuary, Florida, J. Coast. Res., 25(1), 30–47, 2009.

Jaeger, J. M. and Nittrouer, C. A.: A quantitative examination of modern sedimentary lithofacies formation on the glacially influenced Gulf of Alaska continental shelf, Cont. Shelf Res., 26(17), 2178–2204, doi:10.1016/j.csr.2006.07.014, 2006.

Johannessen, S. C. and Macdonald, R. W.: Geoengineering with seagrasses: is credit due where credit is given?, Environ. Res. Lett., 11(11), 113001, doi:10.1088/1748-9326/11/11/113001, 2016.

Johannessen, S. C. and Macdonald, R. W.: Reply to Macreadie et al Comment on " Geoengineering with seagrasses : is credit due where credit is given ?" OPEN ACCESS Reply to Macreadie et al Comment on " Geoengineering with seagrasses : is credit due where credit is given ?," Environ. Res. Lett., 13(2), 28001, doi:10.1088/1748-9326/aaa7b5, 2018.

Kauffman, J. and Donato, D.: Protocols for the measurement, monitoring and reporting of structure, biomass and carbon stocks in mangrove forests, Cent. Int. For., CIFOR work, 40, doi:10.17528/cifor/003749, 2012.

Kelley, J. M., Bond, L. A. and Beasley, T. M.: Global distribution of Pu isotopes and ^{237}Np., Sci. Total Environ., 237, 483–500, 1999.

Kennedy, H., Beggins, J., Duarte, C. M., Fourqurean, J. W., Holmer, M., Marbà, N. and Middelburg, J. J.: Seagrass sediments as a global carbon sink: Isotopic constraints, Global Biogeochem. Cycles, 24(4), 1-9, doi:10.1029/2010GB003848, 2010.

Kirchner, G. and Ehlers, H.: Sediment geochronology in changing coastal environments: Potentials and limitations of the 137Cs and 210Pb methods, J. Coast. Res., 14(1988), 483–492, 1998.

Kirwan, M. and Megonigal, J.: Tidal wetland stability in the face of human impacts and sea-level rise, Nature, 504, 53–60, 2013.

Koch, E.: Beyond light: physical, geological, and geochemical parameters as possible submersed aquatic vegetation habitat requirements, Estuaries, 24(1), 1–17, doi:https://doi.org/10.2307/1352808, 2001.

Koide, M., Soutar, A. and Goldberg, E. D.: Marine geochronology with ^{210}Pb, Earth Planet. Sci. Lett., 14(3), 442–446, doi:10.1016/0012-821X(72)90146-X, 1972.

Krishnaswamy, S., Lal, D., Martin, J. M. and Meybeck, M.: Geochronology of lake sediments, Earth Planet. Sci. Lett., 11(1–5), 407–414, doi:10.1016/0012-821X(71)90202-0, 1971.

Laissaoui, A., Benmansour, M., Ziad, N., Ibn Majah, M., Abril, J. M. and Mulsow, S.: Anthropogenic radionuclides in the water column and a sediment core from the Alboran Sea: Application to radiometric dating and reconstruction of historical water column radionuclide concentrations, J. Paleolimnol., 40(3), 823–833, doi:10.1007/s10933-008-9201-y, 2008.

Li, H. and Yang, S. L.: Trapping Effect of Tidal Marsh Vegetation on Suspended Sediment, Yangtze Delta, J. Coast. Res., 254, 915–924, doi:10.2112/08-1010.1, 2009.

López-Merino, L., Colás-Ruiz, N. R., Adame, M. F., Serrano, O., Martínez Cortizas, A. and Mateo, M. A.: A six thousand-year record of climate and land-use change from Mediterranean seagrass mats, J. Ecol., 105(5), 1267–1278, doi:10.1111/1365-2745.12741, 2017.

Loring, D.: Normalization of heavy-metal data from estuarine and coastal sediments, ICES J. Mar. Sci., 48(1), 101–105, 1991.

Lovelock, C., Ruess, R. and Feller, I.: CO2 efflux from cleared mangrove peat, PLoS One, 6(6), e21279, doi:https://doi.org/10.1371/journal.pone.0021279, 2011.

Lovelock, C. E., Atwood, T., Baldock, J., Duarte, C. M., Hickey, S. and Lavery, P. S.: Assessing the risk of carbon dioxide emissions from blue carbon ecosystems, Front. Ecol. Environ., 15(5), 257–265, doi:10.1002/fee.1491, 2017a.

Lovelock, C. E., Fourqurean, J. W. and Morris, J. T.: Modeled CO2 Emissions from Coastal Wetland Transitions to Other Land Uses: Tidal Marshes, Mangrove Forests, and Seagrass Beds, Front. Mar. Sci., 4, 1–11, doi:10.3389/fmars.2017.00143, 2017b.

Lynch, J. C., Meriwether, J. R., McKee, B. a., Vera-Herrera, F. and Twilley, R. R.: Recent Accretion in Mangrove Ecosystems Based on ^{137}Cs and ^{210}Pb, Estuaries, 12(4), 284, doi:10.2307/1351907, 1989.

Mabit, L., Benmansour, M., Abril, J. M., Walling, D. E., Meusburger, K., Iurian, A. R., Bernard, C., Tarján, S., Owens, P. N., Blake, W. H. and Alewell, C.: Fallout ^{210}Pb as a soil and sediment tracer in catchment sediment budget investigations: A review, Earth-Science Rev., 138, 335–351, doi:10.1016/j.earscirev.2014.06.007, 2014.

Macreadie, P. I., Hughes, A. R., Kimbro, D. L., D'Odorico, P. and McGlathery, K.: Loss of "Blue Carbon" from Coastal Salt Marshes Following Habitat Disturbance, PLoS One, 8(7), e69244, doi:10.1371/journal.pone.0069244, 2013.

Macreadie, P. I., Trevathan-Tackett, S. M., Skilbeck, C. G., Sanderman, J., Curlevski, N., Jacobsen, G. and Seymour, J. R.: Losses and recovery of organic carbon from a seagrass ecosystem following disturbance., Proceedings. Biol. Sci., 282(1817), 20151537, doi:10.1098/rspb.2015.1537, 2015.

Macreadie, P. I., Ewers-Lewis, C. J., Whitt, A. A., Ollivier, Q., Trevathan-Tackett, S. M., Carnell, P. and Serrano, O.: Comment on "Geoengineering with seagrasses: is credit due where credit is given?," Environ. Res. Lett., 13(2), 28002, doi:10.1088/1748-9326/aaa7ad, 2018

Marbà, N., Arias-Ortiz, A., Masqué, P., Kendrick, G. a., Mazarrasa, I., Bastyan, G. R., Garcia-Orellana, J. and Duarte, C. M.: Impact of seagrass loss and subsequent revegetation on carbon sequestration and stocks, J. Ecol., 103, 296–302, doi:10.1111/1365-2745.12370, 2015.

Marland, G., Fruit, K. and Sedjo, R.: Accounting for sequestered carbon: the question of permanence, Environ. Sci. Policy, 4(6), 259–268, doi:10.1016/S1462-9011(01)00038-7, 2001.

Martz, L. and Jong, E. de: Using cesium-137 and landform classification to develop a net soil erosion budget for a small Canadian prairie watershed, Catena, 18(3–4), 289–308, 1991.

Mazarrasa, I., Marbà, N., Lovelock, C. E., Serrano, O., Lavery, P. S., Fourqurean, J. W., Kennedy, H., Mateo, M. a., Krause-Jensen, D., Steven, a. D. L. and Duarte, C. M.: Seagrass meadows as a globally significant carbonate reservoir, Biogeosciences, 12, 4993–5003, doi:10.5194/bg-12-4993-2015, 2015.

Mazarrasa, I., Marbà, N., Garcia-Orellana, J., Masqué, P., Arias-Ortiz, A. and Duarte, C. M.: Effect of environmental factors (wave exposure and depth) and anthropogenic pressure in the C sink capacity of Posidonia oceanica meadows, Limnol. Oceanogr., 62(4), 1436–1450, doi:10.1002/lno.10510, 2017.

McGlathery, K. J., Reynolds, L. K., Cole, L. W., Orth, R. J., Marion, S. R. and Schwarzschild, A.: Recovery trajectories during state change from bare sediment to eelgrass dominance, Mar. Ecol. Prog. Ser., doi:10.3354/meps09574, 2012.

McKee, K. L.: Biophysical controls on accretion and elevation change in Caribbean mangrove ecosystems, Estuar. Coast. Shelf Sci., 91(4), 475–483, doi:10.1016/J.ECSS.2010.05.001, 2011.

Mcleod, E., Chmura, G. L., Bouillon, S., Salm, R., Björk, M., Duarte, C. M., Lovelock, C. E., Schlesinger, W. H. and Silliman, B. R.: A blueprint for blue carbon: toward an improved understanding of the role of vegetated coastal habitats in sequestering CO_2, Front. Ecol. Environ., 9(10), 552–560, doi:10.1890/110004, 2011.

Mudd, S. M., Howell, S. M. and Morris, J. T.: Impact of dynamic feedbacks between sedimentation, sea-level rise, and biomass production on near-surface marsh stratigraphy and carbon accumulation, Estuar. Coast. Shelf Sci., doi:10.1016/j.ecss.2009.01.028, 2009.

Mudd, S. M., D'Alpaos, A. and Morris, J. T.: How does vegetation affect sedimentation on tidal marshes? Investigating particle capture and hydrodynamic controls on biologically mediated sedimentation, J. Geophys. Res. Earth Surf., 115, 1–14, doi:10.1029/2009JF001566, 2010.

Nathwani, J. S. and Phillips, C. R.: Adsorption of ^{226}Ra by soils (I), Chemosphere, 8(5), 285–291, doi:10.1016/0045-6535(79)90111-5, 1979.

Nellemann, C., Corcoran, E. and Duarte, C.M., et al. (eds): Blue carbon. A rapid response assessment, United Nations Environmental Program, GRID-Arendal., 2009.

Oldfield, F. and Appleby, P.: Empirical testing of 210 Pb-dating models for lake sediments, in Lake sediments and environmental history, edited by E. Y. Haworth and W. Lund, Leicester University Press, Leicester, 429, 1984.

Olff, H., Leeuw, J. De, Bakker, J. P., Platerink, R. J. and van Wijnen, H. J.: Vegetation Succession and Herbivory in a Salt Marsh: Changes Induced by Sea Level Rise and Silt Deposition Along an Elevational Gradient, J. Ecol., 85(6), 799, doi:10.2307/2960603, 1997.

Olid, C., Diego, D., Garcia-Orellana, J., Cortizas, A. M. and Klaminder, J.: Modeling the downward transport of 210Pb in Peatlands: Initial Penetration-Constant Rate of Supply (IP-CRS) model, Sci. Total Environ., 541, 1222–1231, doi:10.1016/j.scitotenv.2015.09.131, 2016.

Pendleton, L., Donato, D. C., Murray, B. C., Crooks, S., Jenkins, W. A., Sifleet, S., Craft, C., Fourqurean, J. W., Kauffman, J. B., Marbà, N., Megonigal, P., Pidgeon, E., Herr, D., Gordon, D. and Baldera, A.: Estimating Global "Blue Carbon" Emissions from Conversion and Degradation of Vegetated Coastal Ecosystems, PLoS One, 7(9), 2012.

Preiss, N., Mélières, M.-A. and Pourchet, M.: A compilation of data on lead-210 concentration in surface air and fluxes at the air-surface and water-sediment interfaces, J. Geophys. Res., 101(D22), 28847, doi:10.1029/96JD01836, 1996.

Ravens, T., Thomas, R. and Roberts, K.: Causes of salt marsh erosion in Galveston Bay, Texas, J. Coast. Res., 25(2), 265–272, 2009.

Robbins, J.: Geochemical and geophysical applications of radioactive lead, in The biogeochemistry of lead in the environment, edited by J. Nriagu, Elsevier, Amsterdam, pp. 285–393, 1978.

Robbins, J. A.: A model for particle-selective transport of tracers in sediments with conveyor belt deposit feeders, J. Geophys. Res., 91(C7), 8542, doi:10.1029/JC091iC07p08542, 1986.

Robbins, J. A. and Edgington, D. N.: Determination of recent sedimentation rates in Lake Michigan using Pb-210 and Cs-137, Geochim. Cosmochim. Acta, 39(3), 285–304, doi:10.1016/0016-7037(75)90198-2, 1975.

Ruiz-Fernández, A. C. and Hillaire-Marcel, C.: ^{210}Pb-derived ages for the reconstruction of terrestrial contaminant history into the Mexican Pacific coast: Potential and limitations, Mar. Pollut. Bull., 59(4–7), 134–145, doi:10.1016/j.marpolbul.2009.05.006, 2009.

Sanchez-Cabeza, J. A. and Ruiz-Fernández, A. C.: ^{210}Pb sediment radiochronology: An integrated formulation and classification of dating models, Geochim. Cosmochim. Acta, 82, 183–200, doi:10.1016/j.gca.2010.12.024, 2012.

Sanders, C. J., Smoak, J. M., Sanders, L. M., Waters, M. N., Patchineelam, S. R. and Ketterer, M. E.: Intertidal mangrove mudflat $^{240+239}$Pu signatures, confirming a ^{210}Pb geochronology on the southeastern coast of Brazil, J. Radioanal. Nucl. Chem., 283, 593–596, doi:10.1007/s10967-009-0418-7, 2010a.

Sanders, C. J., Smoak, J. M., Naidu, a. S., Sanders, L. M. and Patchineelam, S. R.: Organic carbon burial in a mangrove forest, margin and intertidal mud flat, Estuar. Coast. Shelf Sci., 90(3), 168–172, doi:10.1016/j.ecss.2010.08.013, 2010b.

Sanders, C. J., Eyre, B. D., Santos, I. R., Machado, W., Luiz-silva, W., Smoak, J. M., Breithaupt, J. L., Ketterer, M. E., Sanders, L., Marotta, H. and Silva-filho, E.: Elevated rates of organic carbon, nitrogen, and phosphorus accumulation in a highly impacted mangrove wetland, Geophys. Res. Lett., 41, 2475–2480, doi:10.1002/2014GL059789, 2014.

Sanders, C. J., Santos, I. R., Maher, D. T., Breithaupt, J. L., Smoak, J. M., Ketterer, M., Call, M., Sanders, L. and Eyre, B. D.: Examining $^{239+240}$Pu, ^{210}Pb and historical events to determine carbon, nitrogen and phosphorus burial in mangrove sediments of Moreton Bay, Australia, J. Environ. Radioact., 151, 623–629, doi:10.1016/j.jenvrad.2015.04.018, 2016.

Serrano, O., Mateo, M. a., Renom, P. and Julià, R.: Characterization of soils beneath a Posidonia oceanica meadow, Geoderma, 185–186, 26–36, doi:10.1016/j.geoderma.2012.03.020, 2012.

Serrano, O., Ruhon, R., Lavery, P. S., Kendrick, G. A., Hickey, S., Masqué, P., Arias-Ortiz, A., Steven, A. and Duarte, C. M.: Impact of mooring activities on carbon stocks in seagrass meadows, Sci. Rep., 6, 23193, doi:10.1038/srep23193, 2016a.

Serrano, O., Ricart, A. M., Lavery, P. S., Mateo, M. A., Arias-Ortiz, A., Masque, P., Rozaimi, M., Steven, A. and Duarte, C. M.: Key biogeochemical factors affecting soil carbon storage in Posidonia meadows, Biogeosciences, 13(15), 4581–4594, doi:10.5194/bg-13-4581-2016, 2016b.

Serrano, O., Davis, G., Lavery, P. S., Duarte, C. M., Martinez-Cortizas, A., Mateo, M. A., Masqué, P., Arias-Ortiz, A., Rozaimi, M. and Kendrick, G. a.: Reconstruction of centennial-scale fluxes of chemical elements in the Australian coastal environment using seagrass archives, Sci. Total Environ., 541, 883–894, doi:10.1016/j.scitotenv.2015.09.017, 2016c.

Sharma, P., Gardner, L. R., Moore, W. S. and Bollinger, M. S.: Sedimentation and bioturbation in a salt marsh as revealed by ^{210}Pb, ^{137}Cs, and ^{7}Be studies, Limnol. Oceanogr., 32(2), 313–326, doi:10.4319/lo.1987.32.2.0313, 1987.

Short, F. T., and Wyllie-Echeverria, S.: Natural and human-induced disturbance of seagrasses, Environ. Conserv., 23(1), 17, doi:10.1017/S0376892900038212, 1996.

Smith, J.: Why should we believe 210Pb sediment geochronologies?, J. Environ. Radioact., 55(2), 121–123, 2001.

Smith, J., Boudreau, B., and Noshkin, V.: Plutonium and ^{210}Pb distributions in northeast Atlantic sediments: subsurface anomalies caused by non-local mixing, Earth Planet. Sci. Lett., 81(1), 15–28, doi:10.1016/0012-821X(86)90097-X, 1986.

Smoak, J. M. and Patchineelam, S. R.: Sediment mixing and accumulation in a mangrove ecosystem : evidence from ^{210}Pb, ^{234}Th and ^{7}Be, Mangroves Salt Marshes, 3, 17–27, http://dx.doi.org/10.1023/A:1009979631884, 1999.

Smoak, J. M., Breithaupt, J. L., Smith, T. J. and Sanders, C. J.: Sediment accretion and organic carbon burial relative to sea-level rise and storm events in two mangrove forests in Everglades National Park, Catena, 104, 58–66, doi:10.1016/j.catena.2012.10.009, 2013.

Sommerfield, C. and Nittrouer, C.: Modern accumulation rates and a sediment budget for the Eel shelf: a flood-dominated depositional environment, Mar. Geol., 154(1–4), 227–241, 1999.

Sun, X., Fan, D., Tian, Y. and Zheng, S.: Normalization of excess ^{210}Pb with grain size in the sediment cores from the Yangtze River Estuary and adjacent areas: Implications for sedimentary processes, The Holocene, 1–13, doi:10.1177/0959683617735591, 2017.

Swales, A. and Bentley, S.: Mangrove-forest evolution in a sediment-rich estuarine system: opportunists or agents of geomorphic change?, Earth Surf. Process. Landforms, 40, 1672–1687, 2015.

Tsabaris, C., Eleftheriou, G. and Kapsimalis, V.: Radioactivity levels of recent sediments in the Butrint Lagoon and the adjacent coast of Albania, Appl. Radiat. Isot., 65(4), 445–453, 2007.

Turner, R. E., Swenson, E. M., Milan, C. S. and Lee, J. M.: Hurricane signals in salt marsh sediments: Inorganic sources and soil volume, Limnol. Oceanogr., 52(3), 1231–1238, doi:10.4319/lo.2007.52.3.1231, 2007.

Walling, D., Collins, A. and Sichingabula, H.: Using unsupported lead-210 measurements to investigate soil erosion and sediment delivery in a small Zambian catchment, Geomorphology, 52(3–4), 193–213, 2003.

Walsh, J. P. and Nittrouer, C. a.: Mangrove-bank sedimentation in a mesotidal environment with large sediment supply, Gulf of Papua, Mar. Geol., 208, 225–248, doi:10.1016/j.margeo.2004.04.010, 2004.

Wan, G. J., Liu, J. and Li, B.: The Isotopic Character and the Remobilization of Lead at the Top of Sediment in Erhai, Chinese Sci. Bull., 38(2), 139–142, doi:10.1360/sb1993-38-2-139, 1993.

Wan, G. J., Chen, J. a., Wu, F. C., Xu, S. Q., Bai, Z. G., Wan, E. Y., Wang, C. S., Huang, R. G., Yeager, K. M. and Santschi, P. H.: Coupling between $^{210}Pb_{ex}$ and organic matter in sediments of a nutrient-enriched lake: An example from Lake Chenghai, China, Chem. Geol., 224, 223–236, doi:10.1016/j.chemgeo.2005.07.025, 2005.

Wentworth, C.: A scale of grade and class terms for clastic sediments, J. Geol., 30(5), 377–392, 1922.

Xu, B., Bianchi, T. S., Allison, M. A., Dimova, N. T., Wang, H., Zhang, L., Diao, S., Jiang, X., Zhen, Y., Yao, P., Chen, H., Yao, Q., Dong, W., Sui, J. and Yu, Z.: Using multi-radiotracer techniques to better understand sedimentary dynamics of reworked muds in the Changjiang River estuary and inner shelf of East China Sea, Mar. Geol., 370, 76–86, doi:10.1016/j.margeo.2015.10.006, 2015.

Yeager, K. and Santschi, P.: Invariance of isotope ratios of lithogenic radionuclides: more evidence for their use as sediment source tracers, J. Environ. Radioact., 69(3), 159–176, 2003.

Yeager, K. M., Brunner, C. a., Kulp, M. a., Fischer, D., Feagin, R. a., Schindler, K. J., Prouhet, J. and Bera, G.: Significance of active growth faulting on marsh accretion processes in the lower Pearl River, Louisiana, Geomorphology, 153–154, 127–143, doi:10.1016/j.geomorph.2012.02.018, 2012.

Biogeosciences Discuss., https://doi.org/10.5194/bg-2018-78
Manuscript under review for journal Biogeosciences
Discussion started: 10 April 2018

Figures, Tables and Boxes

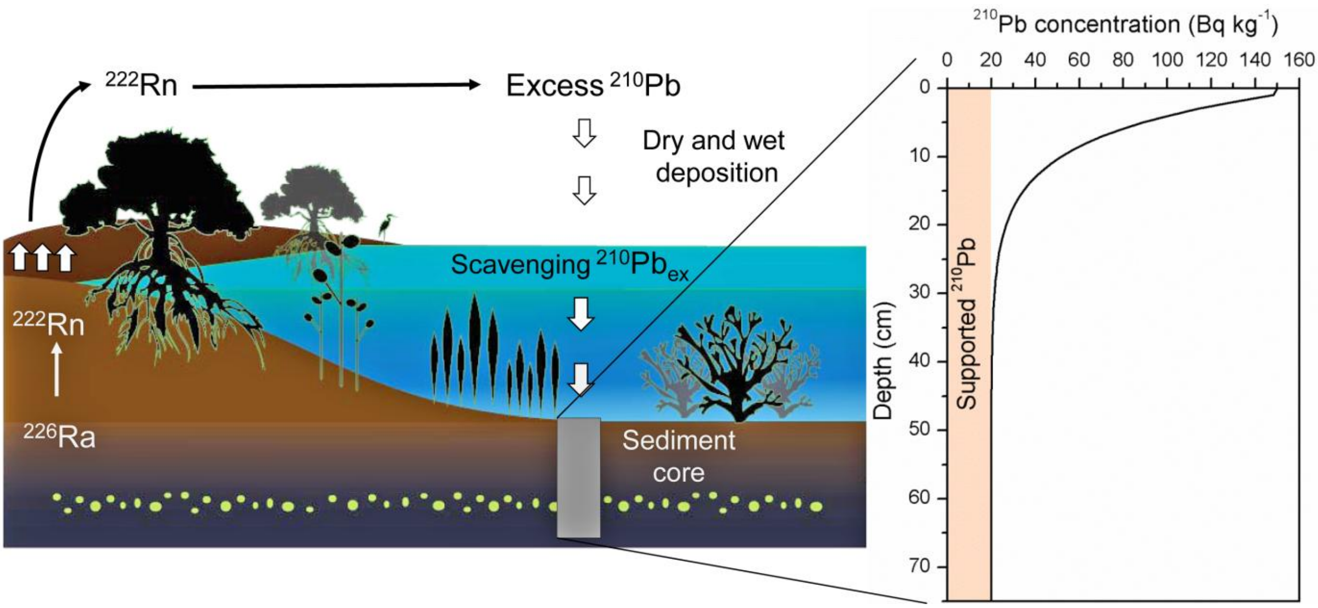

5 **Figure 1. ^{210}Pb cycle and idealized ^{210}Pb concentration profile in sediments.**

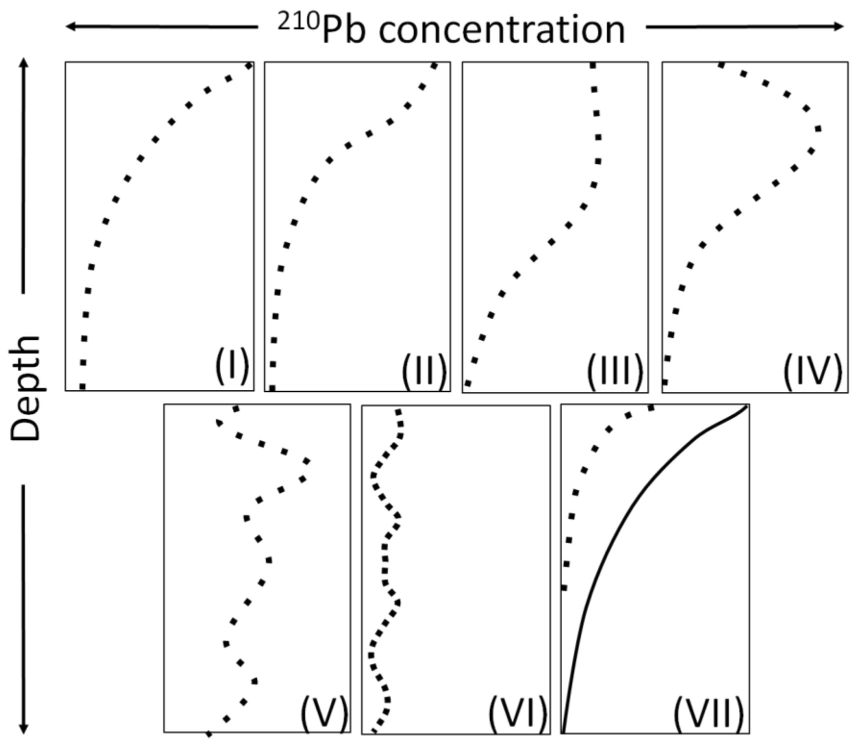

Figure 2. Sketch of seven sedimentary types of excess ^{210}Pb concentration profiles in sediments from vegetated coastal habitats based on a review of the literature. Characteristics of each profile type are explained in the text and summarized in Table 4. The continuous line in Type VII represents the excess ^{210}Pb concentration profile at a reference undisturbed site. Type II (Cearreta et al., 2002; Gardner et al., 1987; Haslett et al., 2003; Swales and Bentley, 2015; Mazarrasa et al., 2017); Type III (Church et al., 1981; Sanders et al., 2010a, 2010b; Serrano et al., 2016a; Sharma et al., 1987; Smoak and Patchineelam, 1999); Type IV (Chen and Twilley, 1999; Greiner et al., 2013; Mudd et al., 2009; Sanders et al., 2010b; Serrano et al., 2016c; Smoak et al., 2013; Yeager et al., 2012); Type V (Alongi et al., 2005; Chanton et al., 1983; Kirchner and Ehlers, 1998; Serrano et al., 2016c; Smoak and Patchineelam, 1999); Type VI (Greiner et al., 2013; Serrano et al., 2016c; 2016d); Type VII (Marbà et al., 2015; Ravens et al., 2009).

Biogeosciences Discuss., https://doi.org/10.5194/bg-2018-78
Manuscript under review for journal Biogeosciences
Discussion started: 10 April 2018

Biogeosciences
Discussions
Open Access

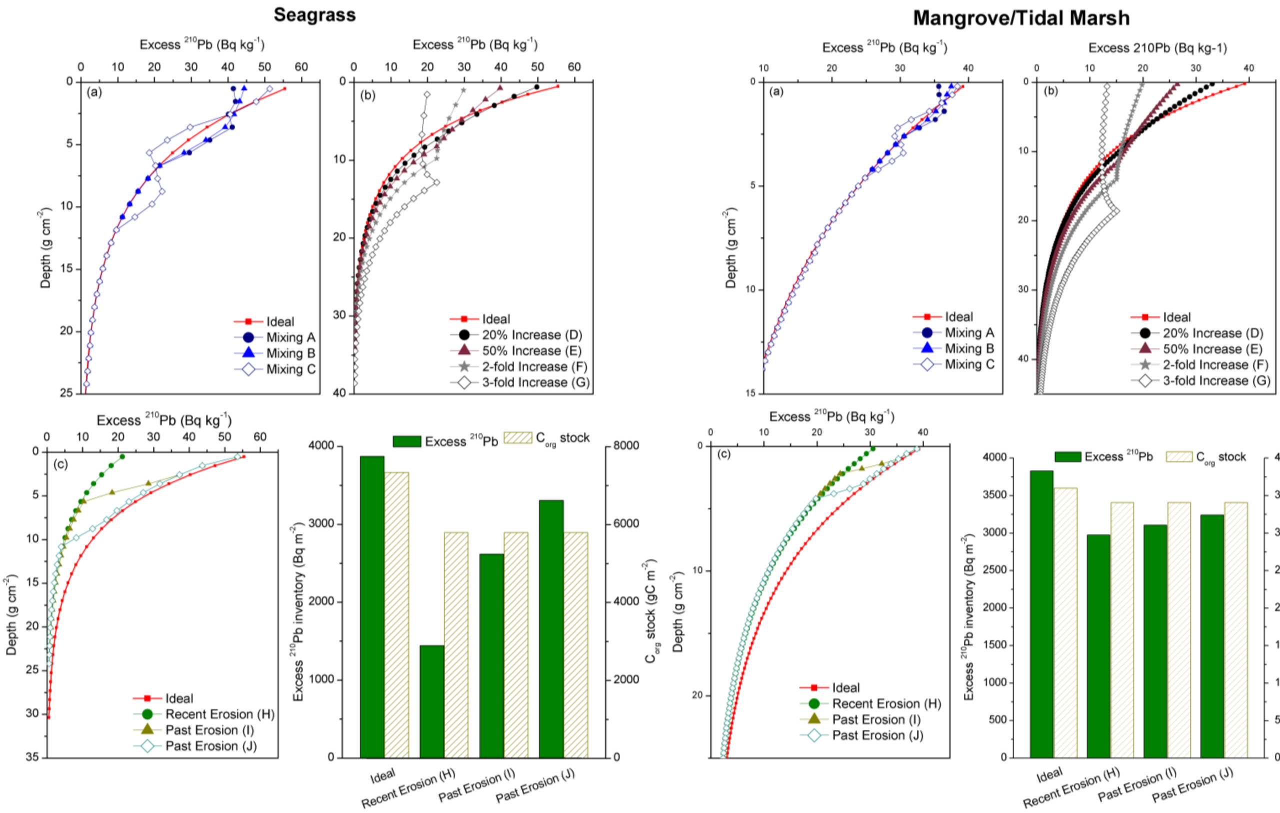

Figure 3. Simulated excess ^{210}Pb concentration profiles of (a) mixing, (b) increase in sedimentation rates and (c) erosion processes in vegetated coastal sediments. Several dry bulk density (DBD) and mass accumulation rates (*MAR*) are used to represent the effects of these processes in seagrass sediments (Left: DBD 1.03 g cm^{-3}; *MAR* = 0.2 g cm^{-2} yr^{-1}; C_{org} = 2.5%) and in mangroves and tidal marsh sediments (Right: DBD: 0.4 g cm^{-3}; *MAR* = 0.3 g cm^{-2} yr^{-1}; C_{org} = 8%). Bar charts illustrate the deficits in excess ^{210}Pb inventories and C_{org} stocks after erosion events. See appendix A for detailed information of each scenario.

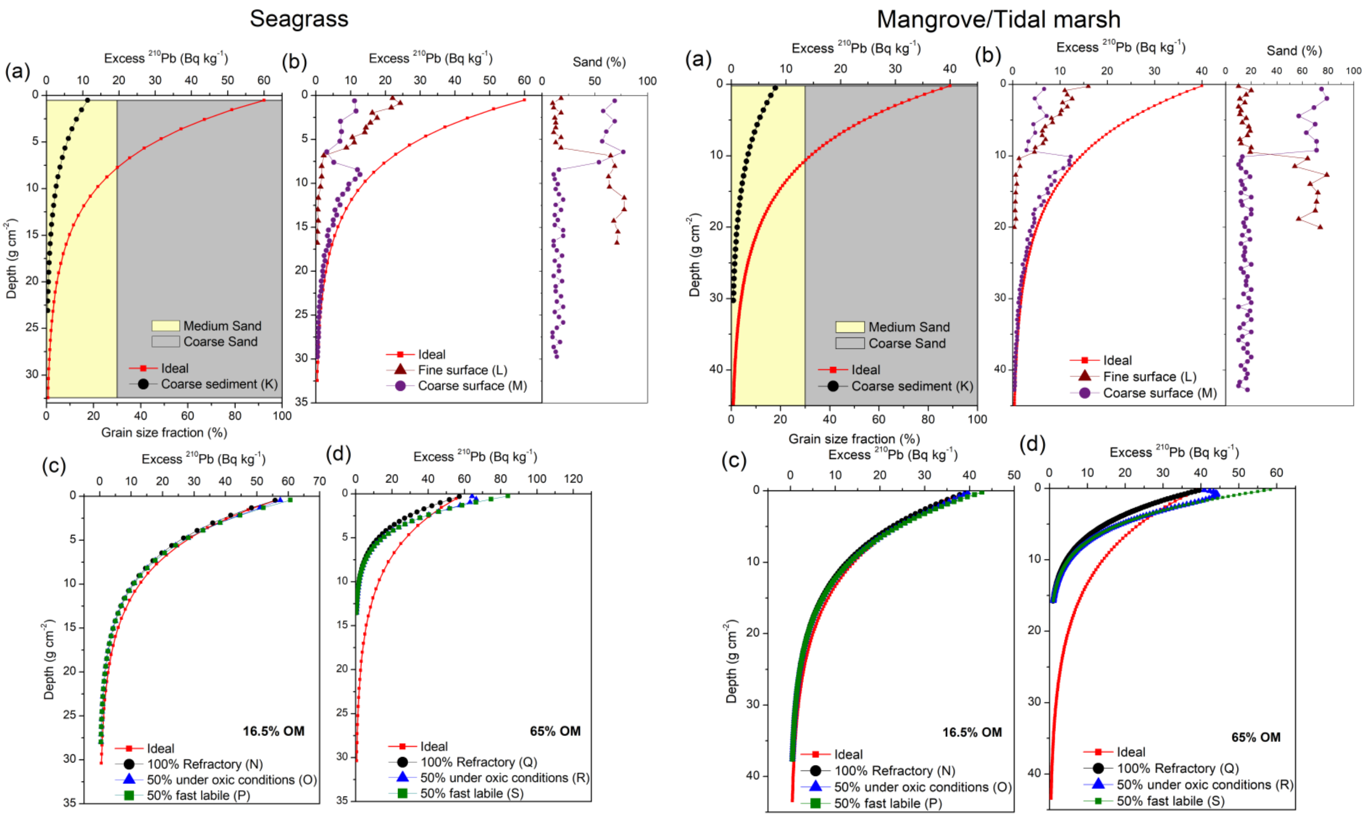

Figure 4. Simulated excess ^{210}Pb concentration profiles of changes in sediment composition and organic matter decay. (a) Coarse homogeneous grain size; (b) heterogeneous grain size with depth, triangles and dots represent an excess ^{210}Pb profile in sediments consisting of fines (< 63 µm) or sands (> 125 µm) at surface layers, respectively; (c and d) organic matter decay from starting level of 16.5% and 65%, respectively (considering different scenarios explained in appendix A) in seagrass (Left: DBD 1.03 g cm^{-3}; MAR = 0.2 g cm^{-2} yr^{-1}) and mangrove/tidal marsh sediments (Right: DBD: 0.4 g cm^{-3}; MAR = 0.3 g cm^{-2} yr^{-1}).

Biogeosciences Discuss., https://doi.org/10.5194/bg-2018-78
Manuscript under review for journal Biogeosciences
Discussion started: 10 April 2018

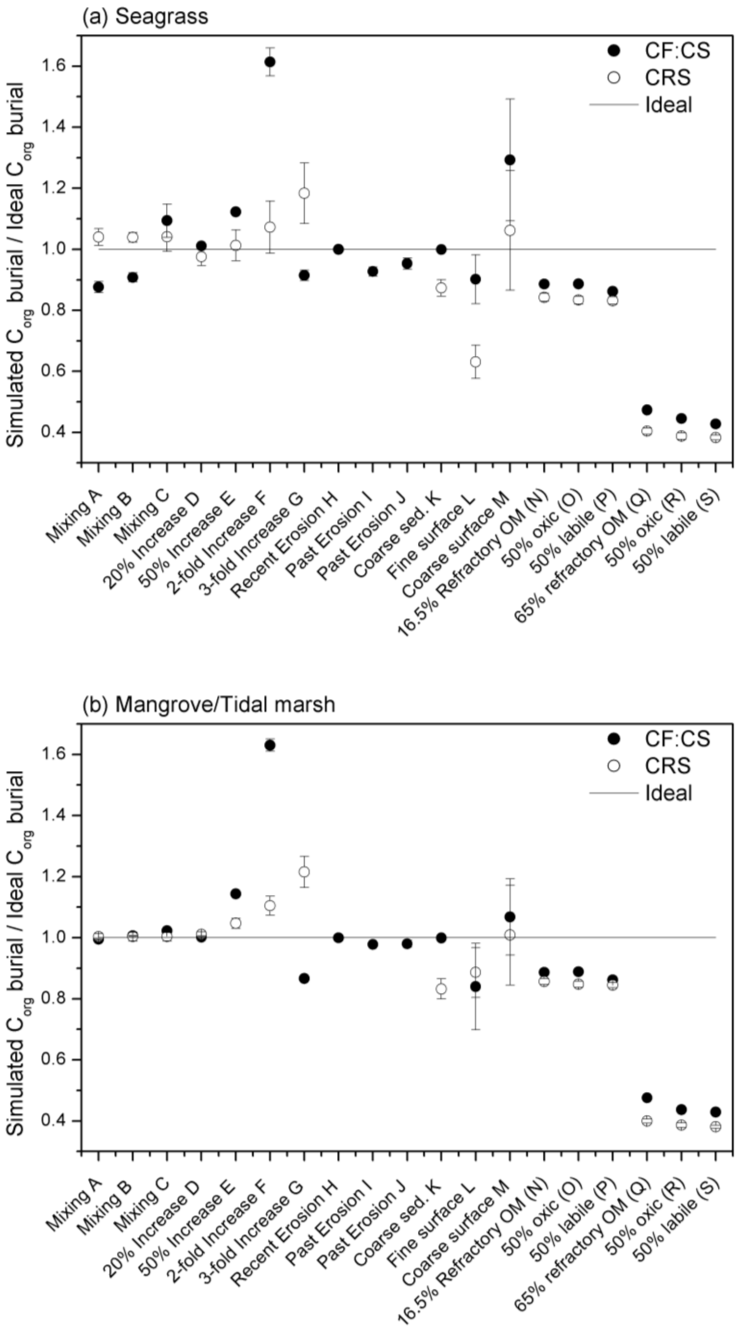

Figure 5. Ratio of C_{org} accumulation rates (C_{org}-MAR) between disturbed and ideal profiles produced by various sedimentary processes. (a) seagrass and (b) mangrove/tidal marsh habitats. Error bars represent SE of the regression and SE of the mean using the CF:CS and CRS models, respectively. C_{org}-MAR could not be estimated in simulations of erosion by means of the CRS model since the excess ^{210}Pb inventory is incomplete. Ratios of simulated/ideal sedimentation rates (MAR) are equal to those of C_{org}-MAR, determined from multiplying MAR by the mean weighed average of C_{org} (Eq. 5). In simulations of increasing sedimentation and organic matter decay, new MAR and C_{org}-MAR were estimated to represent changes in accumulation and higher amounts of organic matter under ideal conditions.

Table 1. Typical values of main parameters of vegetated coastal sediments (seagrass, mangrove and tidal marshes): average dry bulk density (DBD), average sedimentation rates, range of organic matter (OM) content, median organic carbon (C_{org}) contents, and decay rate of buried C_{org} (from above ground biomass to refractory sediment C_{org}).

Habitat Type	DBD[a]	Sediment and mass accumulation rate[b]		OM[c]	C_{org}[d]	Decay rate of buried C_{org}[e]
	($g\ cm^{-3}$)	SAR ($mm\ yr^{-1}$)	MAR ($g\ cm^{-2}\ yr^{-1}$)	(%)	(%)	(d^{-1})
Seagrass	1.03	2.0 ± 0.4	0.21 ± 0.04	0.5-16.5	2.5	0.01- 0.00005
Mangrove	0.45	5.5 ± 0.4	0.25 ± 0.02	7-25	7.0	0.03 – 0.00005
Tidal marsh	0.43	6.7 ± 0.7	0.29 ± 0.03	5-80	9.0	0.005 - 0.00005

[a] Seagrass (Fourqurean et al., 2012); Mangrove (Donato et al., 2011) and Tidal marsh (Craft, 2007; Hatton et al., 1983).
[b] Seagrass and mangrove (Duarte et al., 2013), and tidal marsh (Kirwan and Megonigal, 2013).
[c] Seagrass (Koch, 2001); Mangrove (Breithaupt et al., 2012); Tidal marsh (Cochran et al., 1998; Ember et al., 1987).
[d] Seagrass (Fourqurean et al., 2012); Mangrove (Breithaupt et al., 2012); Tidal marsh (Chmura et al., 2003).
[e] Seagrass, mangrove and tidal marsh (Lovelock et al., 2017b).

Table 2. Summary of the main ^{210}Pb-based models for sediment dating (adapted from Mabit et al., 2014)

Model	Assumptions	Analytical Solutions	References
CIC: Constant Initial Concentration	[1], $\Phi(t)/MAR(t) = Cte$	$C_m = C_0 \cdot e^{-\lambda t}$	(Robbins, 1978; Robbins and Edgington, 1975)
CF:CS: Constant Flux: Constant Sedimentation	[1], [2], [3]	$C_m = C_0 \cdot e^{-\lambda m/MAR};\ t = \frac{m}{MAR}$	(Krishnaswamy et al., 1971)
CRS: Constant Rate of Supply	[1], [2]	$A_m = I \cdot e^{-\lambda t};\ MAR = \frac{\lambda I_m}{C_m}$	(Appleby, 2001; Appleby and Oldfield, 1978)
CMZ:CS Complete Mixing Zone with constant SAR	[2], [3], $k_m = \infty, m \geq m_a$; $k_m = 0, m < m_a$	$C_m = C = \frac{\Phi}{MAR + \lambda m_a}, m \geq m_a$; $C_m = C \cdot e^{-\lambda (m-m_a)/MAR}, m < m_a$	(Robbins and Edgington, 1975)
CF:CS-Constant Diffusion	[2], [3], $k_m = Cte$	$C_m = \frac{\Phi}{MAR - k_m\beta} e^{-\beta m}$; $\beta = \frac{MAR - \sqrt{MAR^2 + 4\lambda k_m}}{2k_m}$	(Laissaoui et al., 2008; Robbins, 1978)
CF:CS-depth dependent diffusion and/or translocational mixing	[2], [3], $k_m = f_m$; may include local sources and sinks	General numerical solution	(Abril, 2003; Abril and Gharbi, 2012; Robbins, 1986; Smith et al., 1986)
IMZ: Incomplete Mixing Zone	[2], [3]	A linear combination of solutions for CF-CS and CMZ-CS with coefficients g and (1 − g), being g ϵ [0, 1]	(Abril et al., 1992)
SIT: Sediment Isotope Tomography	[1]	$C_m = C_0 \cdot e^{-B \cdot m} \cdot e^{\sum_{n=1}^{N} a_n sin\left(\frac{n\pi m}{m_{max}}\right) + \sum_{n=1}^{N} b_n\left(1 - cos\frac{n\pi m}{m_{max}}\right)}$	(Carroll and Lerche, 2003)
NID-CSR: Non-Ideal-Deposition, Constant Sedimentation Rate	[1], [2], [3], fractioning of fluxes, depth distribution	$C_m = C_1 \cdot e^{-\lambda m/MAR} + C_2 \cdot e^{-\alpha m}$; $C_2 = \frac{-\alpha g \Phi}{\alpha MAR - \lambda}$; $C_1 = \frac{(1-g)\Phi}{MAR} - C_2$	(Abril and Gharbi, 2012)
CICCS: constant initial concentration and constant sedimentation rate	[1], [2]	$MAR = \lambda \frac{I - I_{ref}}{C_r}$; I_{ref} = local fallout ^{210}Pb inventory; C_r = Initial excess ^{210}Pb in catchment-derived sediment.	(He and Walling, 1996b)
IP-CRS: Initial Penetration-Constant Rate of Supply	[2], initial mobility of excess ^{210}Pb downward; two compartments 0 to z_k and z_k to ∞	$C_{i\,(z)} = A_i e^{\theta+(i)z} + B_i e^{\theta-(i)z}$; $from\ 0\ to\ z_k$; $C_{i\,(z)} = A_i e^{\sigma+(i)z} + B_i e^{\sigma-(i)z} + \frac{F_i}{\lambda}$; $from\ z_k to\ \infty$; $F_i = \frac{f_i}{(z_i - z_{i-1})} \sum_{m=1}^{k} \int_{z_{m-1}}^{z_m} r_m C_m\, dz$; $\sum f_i = 1$; *See reference for constants*	(Olid et al., 2016)
TERESA: Time estimates from random entries of sediments and	[1], excess ^{210}Pb fluxes are governed by horizontal inputs, correlation with MAR	$C_1 = C_0 \cdot e^{-\lambda T_0} \cdot \frac{1 - e^{-\lambda \Delta T_1}}{\lambda \Delta T_1}$; $C_m = C_0 \cdot e^{-\lambda\left(T_0 + \frac{\Delta_{m-1}}{MAR_{m-1}}\right)} \cdot \frac{1 - e^{-\lambda \Delta T_m}}{\lambda \Delta T_m}$	(Abril, 2016; Botwe et al., 2017)

activities

[1] Non post-depositional redistribution; [2] constant excess ^{210}Pb fluxes at the SWI; [3] constant MAR. All models assume continuity of the sediment sequence.

C_m: excess ^{210}Pb activity concentration in sediments at mass depth m
I: total inventory of excess ^{210}Pb
A_m: excess inventory accumulated below depth m
k_m: effective mixing coefficient ($D\rho^2$)
m_a: mass thickness of top sediment zone
Φ: Flux of excess ^{210}Pb onto the sediment
g: fraction of excess ^{210}Pb flux distributed within a certain mass depth
F_i: additional supply of excess ^{210}Pb to layer *i*

Biogeosciences Discuss., https://doi.org/10.5194/bg-2018-78
Manuscript under review for journal Biogeosciences
Discussion started: 10 April 2018

Biogeosciences Discussions Open Access EGU

Table 3. Summary description of the numerical simulations conducted to test for the effects of sedimentary processes on excess ^{210}Pb concentration profiles in seagrass and mangrove/tidal marsh sediments. k_s is the decay rate of the refractory sediment organic matter (OM) under anoxic conditions and k_{ox} is that in oxic conditions. K_{lb} is the decay constant of the labile OM derived from seagrass and mangrove/tidal marsh ecosystems (0.01 yr^{-1} and 0.03 yr^{-1}, respectively).

Influencing Factor	Scenario	Description
Mixing	A	Random upper 5 cm
	B	Random upper 5 cm
	C	Random upper 5-10 cm
Increasing sedimentation	D	Increased basal MAR by 20%
	E	Increased basal MAR by 50%
	F	Increased basal MAR by 200%
	G	Increased basal MAR by 300%
Erosion	H	Removal of excess ^{210}Pb inventory from 0-5 cm
	I	Removal of excess ^{210}Pb inventory from 5-10 cm
	J	Removal of excess ^{210}Pb inventory from 10-15 cm
Grain size	K	Coarse sediment (70% coarse, 30% medium)
	L	Fine surface sediments (10 - 20% of sands at surface)
	M	Coarse surface sediments (40 - 80% of sands at surface)
Organic matter		16.5% OM
	N	100% with: ks = 0.00005 d^{-1}
	O	50% with *kox* = 0.0005 d^{-1}
	P	50% with k_{lb} = 0.01 d^{-1} or 0.03 d^{-1}
		65% OM
	Q	100% with: ks = 0.00005 d^{-1}
	R	50% with *kox* = 0.0005 d^{-1}
	S	50% with k_{lb} = 0.01 d^{-1} or 0.03 d^{-1}

Biogeosciences Discuss., https://doi.org/10.5194/bg-2018-78
Manuscript under review for journal Biogeosciences
Discussion started: 10 April 2018

Table 4. Diagnostic features for seven distinct styles of sediment accumulation in vegetated coastal sediments (based on excess ^{210}Pb concentration profiles as shown in Figure 2) and recommended actions to interpret the ^{210}Pb profiles and the sedimentary processes most likely involved.

Type	Profile description	Most likely sedimentation process	Action
I	Excess ^{210}Pb concentrations declining exponentially	Steady-state accumulation	• Use independent tracers to validate chronology.
II	Shift in the slope of excess ^{210}Pb concentrations	Mixing (physical or bioturbation)	• Check if profiles of other elements or parameters are homogeneous. • Analyse short-lived radionuclides at the SML. • Check for burrowing evidence. • X-ray radiographs and CAT-scans. • CRS model or CF:CS model below SML (check residence time of excess ^{210}Pb in the mixed layer).
		Change in sedimentation rate	• Use independent tracers to validate MAR in regions with different slope. • Check distribution of chemical elements, grain size or geochemical information. • Check historical records of natural events or human impacts in the area. • Apply CRS or CF:CS model piecewise.
		Changes in sediment composition	• Check grain size distribution, DBD and OM content profiles. • Normalize radionuclide concentrations to < 63 µm, OM, trace metals such as Al. • Analyze ^{226}Ra in all sections. • CF:CS dating model if no actions are taken.
		Past erosion	• Compare excess ^{210}Pb inventories with those at a reference site. • Grain size analysis at both reference and eroded sites. • CF:CS model to estimate MAR.

III	Surface mixed layer (SML) overlying exponentially decaying excess ^{210}Pb concentration profile	Mixing (physical or bioturbation)	• Check if profiles of other elements or parameters are homogeneous. • Analyse short-lived radionuclides at the SML. • Check for suitable burrowing community. • X-ray radiographs and CAT-scans. • CRS model or CF:CS model below SML (check residence time of excess ^{210}Pb in the mixed layer).
		Acceleration of sedimentation	• Use independent tracers to validate MAR in regions with different slope. • Check variations in grain size, OM or water content or geochemical information. • Test sensitivity to acceleration according to DBD and apparent sedimentation rate. • Check historical records of natural events or human impacts in the area. • Apply CRS or CF:CS model piecewise.
		Organic matter decay	Only if %OM is very high (>30%) and mostly labile.
IV	Reverse ^{210}Pb pattern indicating dilution of surface excess ^{210}Pb concentrations	Mixing (physical or bioturbation)	• Check if profiles of other elements or parameters are homogeneous. • Analyse short-lived radionuclides at the SML. • Check for burrowing evidence. • X-ray radiographs and CAT-scans. • CRS model or CF:CS model below SML (check residence time of excess ^{210}Pb in the mixed layer).
		Acceleration of sedimentation	• Use independent tracers to validate MAR in regions with different slope. • Check variations in grain size, OM, water content or geochemical information. • Test sensitivity to acceleration according to DBD and apparent sedimentation rate. • Check historical records of natural events or human impacts in the area. • Apply CRS or CF:CS model piecewise.

		Recent coarse sediment deposition	• Check grain size distribution, DBD and water content profiles. • Normalize radionuclide concentrations to < 63 µm or to OM content. • Analyze ^{226}Ra in all sections. • Historical records of event sedimentation or erosion. • CF:CS dating model if no actions are taken.
		Organic matter decay	Only if %OM is very high (>30%) and mostly labile.
V	Stair-stepped excess ^{210}Pb profile	Heterogeneous sediment composition	• Check grain size distribution, DBD and OM content profiles. • Normalize radionuclide concentrations to < 63 µm, to OM content or to trace metals such as Al. • Analyze ^{226}Ra in all sections. • CF:CS dating model if no actions are taken.
		Periodic repetition of physical or biological mixing	• Analyse short-lived radionuclides along the mixed region. • Check for burrowing evidence. • X-ray radiographs, CAT-scans. • Estimation of inventories. • Maximum MAR estimated by the penetration-depth method.
		Rapid sediment accumulation rate	• Analyse short-lived radionuclides. • Analyze ^{226}Ra if supported ^{210}Pb is not reached.
VI	Low and constant excess ^{210}Pb activities with depth, showing low, negligible modern accumulation	Erosion	• Compare excess ^{210}Pb inventories with those at a reference site. • Grain size analysis at both reference and eroded sites. • Check presence of short-lived radionuclides at reference site.
		Coarse sediment composition	• Analyse radionuclides in the fine sediment fraction (sieve to < 63 or < 125 µm).
VII	Excess ^{210}Pb concentrations and inventories << than those of reference site	Erosion	• Compare excess ^{210}Pb inventories with those at a reference site. • Grain size analysis at both ref. and eroded site. • Check presence of short-lived radionuclides at reference site.

Biogeosciences Discuss., https://doi.org/10.5194/bg-2018-78
Manuscript under review for journal Biogeosciences
Discussion started: 10 April 2018

Box 1. Case Study of Mixing

An example of bioturbation processes is documented by Smoak and Patchineelam (1999) where they showed a mixed excess ^{210}Pb profile down to 11 cm depth in a mangrove ecosystem in Brazil evidenced from the ^{210}Pb, ^{234}Th and ^{7}Be concentration profiles. The excess ^{210}Pb concentration decreases exponentially below the surface mixed layer, resulting in an estimated accumulation rate of 1.8 mm yr^{-1}. In the upper layers the excess ^{210}Pb follows a complex pattern, with alternate relative maxima and minima, which could be representative of varying conditions of fluxes and sediment accumulation rates, presence of coarse sediments or physical or biological mixing. However, ^{7}Be penetrated down to 4 cm depth and excess ^{234}Th was detected only in the surface layer. Sediments that are buried for a period of more than 6 months will have undetectable ^{7}Be, hence its presence at 4 cm depth indicated that the activity of benthic communities had remobilised it downwards to a much greater degree than sedimentation.

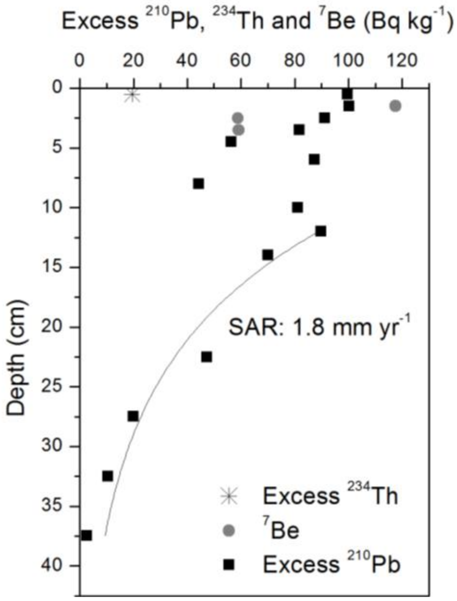

Panel A. Excess ^{210}Pb concentration profile affected by bioturbation. Short-lived ^{7}Be and excess ^{234}Th concentration profiles are indicators of mixing in the zone of constant excess ^{210}Pb concentrations (0 - 5 cm). (Adapted from Smoak and Patchineelam, (1999).

Box 2. Case Study of rapid sedimentation rates

Alongi et al. (2005) studied the rates of sediment accumulation at three mangrove forests spanning the intertidal zone along the south coastline of the heavily urbanized Jiulongljiang Estuary (China). Mass accumulation rates (MAR) were rapid and one of the excess ^{210}Pb concentration profiles showed scattered concentrations with depth. This could be related to either a very high MAR during the last decades or a very intense mixing down core. However, the excess ^{228}Th concentration profile, determined from the difference between the total ^{228}Th and ^{228}Ra concentrations in the sediment, showed a clearly decaying trend down to 15 cm (Panel B). The exponential decay curve fitted to the excess ^{228}Th concentrations yielded an accumulation rate of 10 cm yr^{-1}, which was consistent with the ^{210}Pb concentration profile. Therefore, the evidence provided by excess ^{228}Th indicated that a very high MAR was the most plausible processes responsible for the sediment record.

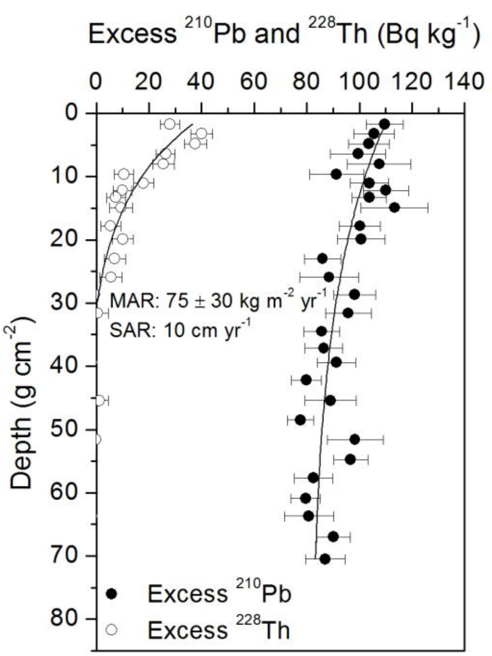

Panel B. Vertical concentration profiles of excess ^{210}Pb and ^{228}Th in core 3564 fom Alongi et al. (2005), produced by a rapid mass accumulation rate.

Box 3. Case study of a sedimentation event

Hurricanes and cyclones can lead to the sudden delivery of large amounts of sediments and nutrients to mangroves and tidal marshes, which in turn can result in enhanced production (Castañeda-Moya et al., 2010; Lovelock et al., 2011). Smoak et al. (2013) obtained an excess ^{210}Pb concentration profile consistent with a large pulse of sediment delivered to fringing mangroves in the Everglades, Florida (Panel C). The concentration of excess ^{210}Pb was vastly different (several times lower) in sediments accumulated during the event. The estimated sediment accumulation rate estimated by the CRS model for the upper part of the sediment record was six times that of background levels, resulting in a doubled accretion rate, due to the high bulk density of the delivered sediments (Castañeda-Moya et al., 2010). C_{org} concentrations in the abruptly accumulated sediments were lower (5%) than those of the sediments beneath the event layer (20-25%).

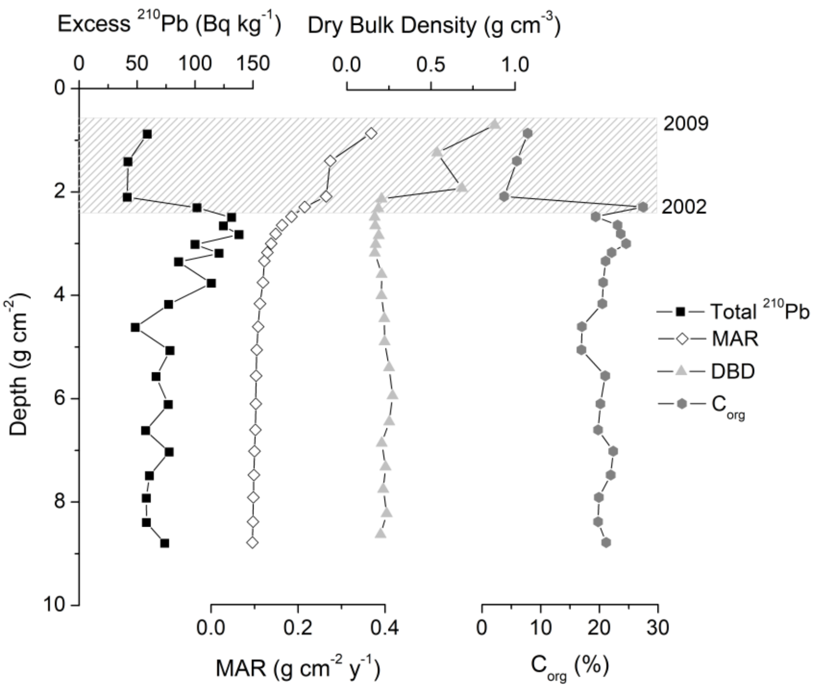

Panel C. Excess ^{210}Pb, mass sedimentation rates (MAR), dry bulk density and C_{org} content in a mangrove sediment core at the Everglades, Florida. The gridded area represents the period 2002 - 2009, when Hurricane Wilma (2005) delivered a large pulse of sediment (Adapted from Smoak et al., 2013).

Box 4. ^{226}Ra (supported ^{210}Pb) variation with depth

The ^{210}Pb, ^{226}Ra and grain size profiles in panel D illustrate an example of a seagrass sediment core collected from Carnarvon, Western Australia, where the sediment record contained low total ^{210}Pb concentrations and had a heterogeneous grain size distribution, leading to a variability in ^{226}Ra concentrations of up to 4-fold (from 7 - 31 Bq kg^{-1}). Low ^{210}Pb concentrations might result from high contents of coarse sediments or regional characteristics such as low atmospheric excess ^{210}Pb fluxes. ^{210}Pb atmospheric flux varies spatially depending upon rainfall (wash out frequency) or geographical location (^{222}Rn sources, i.e., land masses) (Preiss et al., 1996). Due to the continental or oceanic origin of air masses, there is a consistent west to east increase in excess ^{210}Pb fallout within the major continents. Carnarvon, located in the Southern Hemisphere and mostly influenced by winds which have an oceanic origin low excess ^{210}Pb fluxes occur (Preiss et al., 1996).

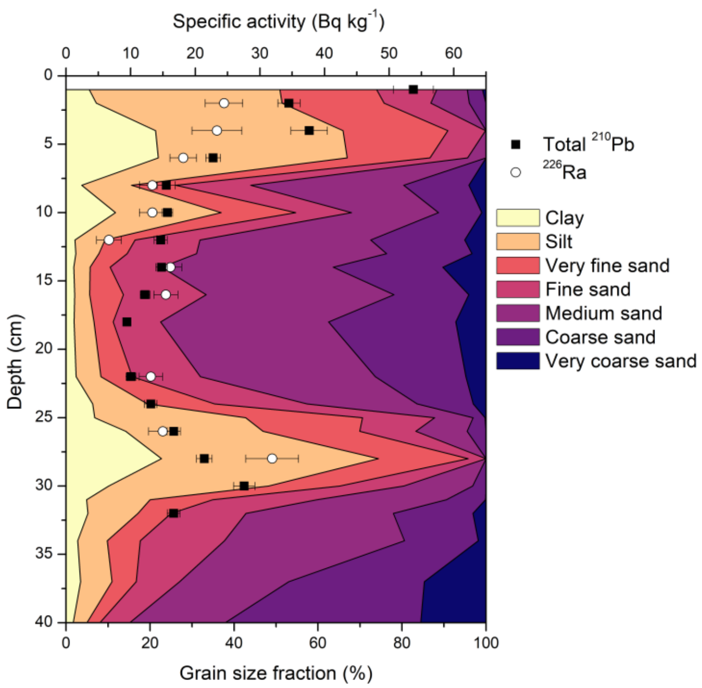

Panel D. Total ^{210}Pb and ^{226}Ra concentration profiles superimposed on grain size distribution in a seagrass sediment core in Carnarvon, Western Australia (unpublished data).

Box 5. Case Study of Erosion

Incomplete inventories of excess ^{210}Pb indicative of erosion can be illustrated by the measured ^{210}Pb concentration profiles in sediments from Oyster Harbor (Albany, Western Australia), some of which were devoid of seagrass vegetation since the 1980s due to eutrophication (Marbà et al., 2015). The measured excess ^{210}Pb concentrations in the unvegetated sediments were relatively low, and the horizons of excess ^{210}Pb were detected at shallower sediment depths than in neighboring sediments, where seagrass meadows persisted (Panel E). The inventory of excess ^{210}Pb in the unvegetated sediment exhibited a deficit of 722 Bq m^{-2} compared to that in the vegetated site. This deficit could not solely result from the lack of accumulation of excess ^{210}Pb while sediments were unvegetated (30 years; atmospheric flux of 25 Bq m^{-2} yr^{-1}), but also to the subsequent sediment erosion. These results, combined with C_{org} analyses, showed that unvegetated sediments had an average deficit in accumulated C_{org} stocks of 2.3 kg C_{org} m^{-2} compared to vegetated sediments over the last ca. 100 years. This deficit was produced since seagrass loss in 1980, but was equivalent to a loss of approximately 90 years of C_{org} accumulation.

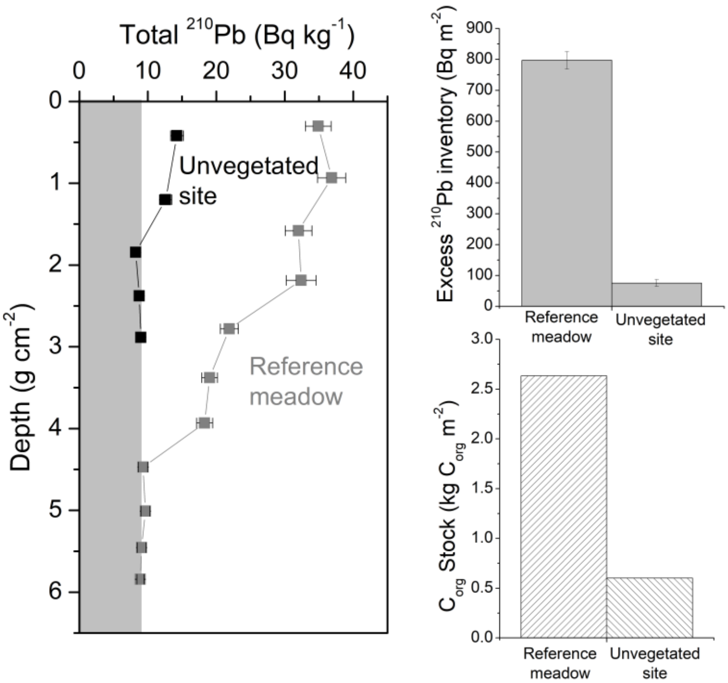

Panel E. Comparison of ^{210}Pb concentration profiles and inventories of excess ^{210}Pb and organic carbon (C_{org}) between vegetated and unvegetated site. The grey area indicates supported ^{210}Pb concentrations (Adapted from Marbà et al., 2015).